OPEN ACCESS Freely available online

PLoS PATHOGENS

The Coxsackievirus B 3C^{pro} Protease Cleaves MAVS and TRIF to Attenuate Host Type I Interferon and Apoptotic Signaling

Amitava Mukherjee[1], Stefanie A. Morosky[2], Elizabeth Delorme-Axford[1], Naomi Dybdahl-Sissoko[3], M. Steven Oberste[3], Tianyi Wang[4], Carolyn B. Coyne[2]*

1 Department of Cell Biology and Physiology, University of Pittsburgh, Pittsburgh, Pennsylvania, United States of America, **2** Department of Microbiology and Molecular Genetics, University of Pittsburgh, Pittsburgh, Pennsylvania, United States of America, **3** Picornavirus Laboratory, Centers for Disease Control and Prevention, Atlanta, Georgia, United States of America, **4** Department of Infectious Diseases and Microbiology, University of Pittsburgh, Pittsburgh, Pennsylvania, United States of America

Abstract

The host innate immune response to viral infections often involves the activation of parallel pattern recognition receptor (PRR) pathways that converge on the induction of type I interferons (IFNs). Several viruses have evolved sophisticated mechanisms to attenuate antiviral host signaling by directly interfering with the activation and/or downstream signaling events associated with PRR signal propagation. Here we show that the 3C^{pro} cysteine protease of coxsackievirus B3 (CVB3) cleaves the innate immune adaptor molecules mitochondrial antiviral signaling protein (MAVS) and Toll/IL-1 receptor domain-containing adaptor inducing interferon-beta (TRIF) as a mechanism to escape host immunity. We found that MAVS and TRIF were cleaved in CVB3-infected cells in culture. CVB3-induced cleavage of MAVS and TRIF required the cysteine protease activity of 3C^{pro}, occurred at specific sites and within specialized domains of each molecule, and inhibited both the type I IFN and apoptotic signaling downstream of these adaptors. 3C^{pro}-mediated MAVS cleavage occurred within its proline-rich region, led to its relocalization from the mitochondrial membrane, and ablated its downstream signaling. We further show that 3C^{pro} cleaves both the N- and C-terminal domains of TRIF and localizes with TRIF to signalosome complexes within the cytoplasm. Taken together, these data show that CVB3 has evolved a mechanism to suppress host antiviral signal propagation by directly cleaving two key adaptor molecules associated with innate immune recognition.

Citation: Mukherjee A, Morosky SA, Delorme-Axford E, Dybdahl-Sissoko N, Oberste MS, et al. (2011) The Coxsackievirus B 3C^{pro} Protease Cleaves MAVS and TRIF to Attenuate Host Type I Interferon and Apoptotic Signaling. PLoS Pathog 7(3): e1001311. doi:10.1371/journal.ppat.1001311

Editor: Mark Heise, University of North Carolina at Chapel Hill, United States of America

Received June 23, 2010; **Accepted** February 2, 2011; **Published** March 10, 2011

This is an open-access article distributed under the terms of the Creative Commons Public Domain declaration which stipulates that, once placed in the public domain, this work may be freely reproduced, distributed, transmitted, modified, built upon, or otherwise used by anyone for any lawful purpose.

Funding: This work was supported by funding from the NIH [R01AI081759 (CBC)]. The funders had no role in study design, data collection and analysis, decision to publish, or preparation of the manuscript.

Competing Interests: The authors have declared that no competing interests exist.

* E-mail: coynec2@pitt.edu

Introduction

The innate immune system is the first line of defense against pathogen infiltration and is activated by the binding of conserved microbial ligands to pattern recognition receptors (PRRs). Activation of these receptors culminates in nuclear factor (NF)-κB and/or IFN regulatory factor (IRF)-mediated induction of type 1 interferons (IFN-α and -β), key components of antimicrobial host defenses.

PRRs, including Toll-like receptors (TLRs) and DExD/H box RNA helicases, signal through an assortment of downstream adaptor molecules to propagate innate immune signaling. TLRs signal through adaptor molecules such as myeloid differentiation factor 88 (MyD88), Toll/IL-1 receptor domain containing adaptor protein (TIRAP), Toll/IL-1 receptor domain containing adaptor inducing interferon-beta (TRIF), and TRIF-related adaptor molecule (TRAM) to activate cellular defenses [1]. These adaptors often display specificity with regard to the TLR family members with whom they interact with and from which they are activated. The specificity of TLR ectodomain-ligand recognition and concomitant specificity in the signaling networks that are engaged by this interaction provides an efficient strategy for microbial recognition. In contrast, activated DExD/H box RNA helicases, which include melanoma differentiation associated gene (MDA5) and retinoic acid induced gene-I (RIG-I), signal to a common downstream adaptor molecule, mitochondrial antiviral signaling [(MAVS), also known as VISA/IPS-1/Cardif] to activate NFκB and IRF3 [2,3,4]. MAVS is localized to the mitochondrial membrane and to peroxisomes via a C-terminal transmembrane domain, which is essential for innate immune signaling [5,6]. PRR-associated adaptor molecules thus serve critical roles in the activation of cellular defenses associated with microbial recognition.

As host cells have developed highly specialized strategies for microbial detection and clearance, it is not surprising that many viruses have evolved strategies to counter these defenses in order to promote their replication and spread. In some cases, virally-encoded proteases directly target components of the innate immune system to abolish antiviral signaling via TLRs and/or DExD/H box helicases. Targeted proteolysis of adaptor molecules serves as a powerful means to eliminate antiviral signaling by suppressing common downstream targets of key innate immune signaling pathways. For example, MAVS is cleaved by the NS3/4A serine protease of hepatitis C virus (HCV) [7], the 3C^{pro} cysteine protease of hepatitis A virus (HAV) [8], the HCV-related GB virus B NS3/4A protease [9], and the 2A^{pro} and 3C^{pro} proteases of rhinovirus [10]. HCV also utilizes the same NS3/4A serine protease to cleave TRIF in order to silence TLR3-mediated

Author Summary

Mammalian cells utilize a variety of defenses to protect themselves from microbial pathogens. These defenses are initiated by families of receptors termed pattern recognition receptors (PRRs) and converge on the induction of molecules that function to suppress microbial infections. PRRs respond to essential components of microorganisms that are broadly expressed within classes of pathogens. The relative non-specificity of this detection thus allows for a rapid antimicrobial response to a variety of microorganisms. Coxsackievirus B3 (CVB3), a member of the enterovirus genus, is associated with a number of diverse syndromes including meningitis, febrile illness, diabetes, and is commonly associated with virus-induced heart disease in adults and children. Despite its significant impact on human health, there are no therapeutic interventions to treat CVB3 infections. Here we show that CVB3 has evolved an effective mechanism to suppress PRR signal propagation by utilizing a virally-encoded protein, termed $3C^{pro}$, to directly degrade molecules that function downstream of PRR signaling. By targeting these molecules, CVB3 can evade host detection and escape antiviral defenses normally induced by mammalian cells. These findings will lead to a better understanding of the mechanisms employed by CVB3 to suppress host antiviral signaling and could lead to the development of therapeutic interventions aimed at modulating CVB3 pathogenesis.

signaling [11]. Thus, the targeting of MAVS and/or TRIF by virally-encoded proteases in order to suppress antiviral signaling is emerging as a common theme in the evasion of host defenses.

Enteroviruses, which belong to the *Picornaviridae* family, are small single-stranded RNA viruses that account for several million symptomatic infections in the United States each year. Coxsackievirus B3 (CVB3), a member of the *Enterovirus* genus, is associated with a number of diverse syndromes, including meningitis, febrile illness, and diabetes [12] and is an important causative agent of virus-induced heart disease in adults and children [13,14,15,16]. The induction of type I IFN signaling is essential for the control of CVB3 infection, as evidenced by enhanced virus-induced lethality in type I IFN receptor (IFN-$\widetilde{\alpha}\beta$ R) null mice [17] and increased susceptibility to CVB3 infection in IFNβ-deficient mice [18]. Both TLR3- and MDA5-mediated type I IFN signaling have been implicated in the response to CVB3 infections and mice deficient in either TRIF or MAVS show an enhanced susceptibility to viral infection [19,20,21].

In this study, we determined the potential mechanisms employed by CVB3 to antagonize type I IFN signaling. We found that infection of cells with CVB3 led to the cleavage of the adaptor molecules MAVS and TRIF. Both MAVS and TRIF were cleaved by the CVB3-encoded cysteine protease $3C^{pro}$, indicating that a single protease suppresses innate immune signaling through two powerful pathways. We found that $3C^{pro}$ cleaves specific residues within MAVS and TRIF that render these molecules deficient in type I IFN signaling and apoptotic signaling. Taken together, these data suggest that CVB3 has evolved a mechanism to cleave adaptor components of the innate immune system to escape host immunity.

Results

CVB3 infection does not induce IRF3 nuclear localization or significant type I IFN responses

The induction of type I IFNs is the earliest cellular immune response initiated to combat viral infections and is coordinated by the activation of transcription factors such as interferon regulatory factor (IRF)-3, IRF7, and NFκB downstream of PRR activation. We found that CVB3 infection of HEK293 cells led to only a modest induction of IRF3 activation as assessed by immunofluorescence microscopy for nuclear translocation (Figure 1A), western blot analysis of nuclear extracts (Figure 1B), and luciferase activity assays for IFNβ (Figure 1C). In contrast, transfection of cells with poly I:C induced pronounced IRF3 activation (Figure 1A–C). We also observed little activation of NFκB signaling in response to CVB3 infection as determined by luciferase activation assay (Figure 1C).

Because CVB3 did not elicit a pronounced translocation of IRF3 into the nucleus during infection of HEK293 cells, we investigated the role of several PRRs in mediating CVB3 recognition–TLR3, RIG-I, and MDA5. Both MDA5 [22] and TLR3 [19] have been proposed to act as sensors for CVB3 infection. Although infection of cells with CVB3 is sensitive to IFNβ (Supplemental Figure S1A), we observed less enhancement of IFNβ promoter activity as assessed by luciferase activation in CVB3-infected HEK293 cells overexpressing MAVS, MDA5, RIG-I, and TLR3/TRIF than in uninfected controls (Figure 1D). Instead, we observed the partial ablation of IFNβ promoter activity in response to ectopic expression of MAVS, RIG-I, MDA5, and TLR3/TRIF in CVB3 infected cells (Figure 1D). We also found that CVB did not induce potent IFNβ production in HEK293, HeLa, or Caco-2 cells in comparison to VSV controls (Figure 1E).

MAVS and TRIF are cleaved in CVB3-infected cells

Because CVB3 infection was inefficient at inducing IRF3, we assessed the pattern of expression of MAVS in CVB3-infected HEK293 cells. By immunoblot analysis, we found that CVB3 infection induced the cleavage of MAVS (Figure 2A). Similar results were obtained in HeLa cells (Supplemental Figure S2A). This effect was specific for CVB3 as infection with VSV did not alter MAVS migration (Supplemental Figure S2B). In uninfected cells, full-length MAVS migrated as a single band of ~75 kD. However, in cells infected with CVB3, there was a decrease in the expression level of full-length MAVS and the appearance of a distinct MAVS cleavage fragment migrating at ~40–50 kD (Figure 2A). Because MAVS cleavage is induced in cells undergoing apoptosis [23,24] and CVB3 is known to induce apoptosis in many cell types [25,26], we investigated the role of apoptosis in CVB3-induced MAVS cleavage. We found that incubation of CVB3-infected HEK293 cells with the broad caspase inhibitor z-VAD-FMK and the proteosome inhibitor MG132 had little effect on CVB3-induced MAVS cleavage (Figure 2A). (The slight reduction in MAVS cleavage observed in the presence of MG132 is likely attributable to a reduction in replication in MG132-exposed cells, consistent with previously published results [27,28]). The kinetics of MAVS cleavage was also not consistent with apoptosis: MAVS cleavage was evident by 3 hrs post-infection (p.i.) whereas apoptosis (as measured by caspase-3 cleavage) did not occur until 5–6 hrs p.i. (Figure 2B).

MAVS is localized to the mitochondrial membrane via a C-terminal transmembrane domain [5]. We found that CVB3 infection induced a pronounced decrease in MAVS mitochondrial localization as assessed by immunofluorescence microscopy with a mitochondrial marker (Figure 2C). We also found that the expression and mitochondrial localization of ectopically expressed MAVS was significantly reduced in CVB3-infected cells (Figure 2D, 2E). The appearance of cleavage fragments was evident in CVB3-infected cells overexpressing MAVS (Figure 2D). Moreover, we found that mutation of the caspase cleavage site of

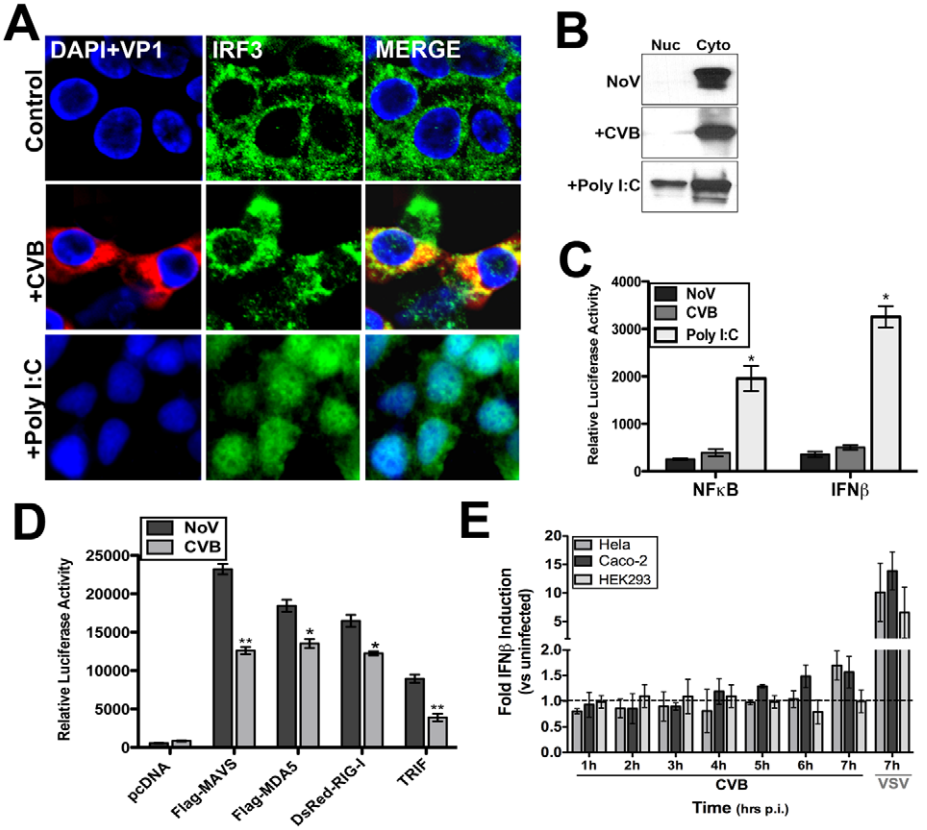

Figure 1. CVB3 infection does not induce significant type I IFN responses. HEK293 cells were infected with CVB3 (1 PFU/cell) for 8 hrs or treated with poly I:C conjugated to transfection reagent [poly I:C/LyoVec (100 ng/mL)] for 12 hrs and (**A**) fixed and stained for virus (VP1, red) and IRF3 (green) or (**B**) western blot analysis for IRF3 performed on nuclear and cytoplasmic fractions. (**C**) Luciferase assays (expressed in relative luciferase activity) from HEK293 cells transfected with NFκB and IFNβ promoted luciferase constructs and infected with CVB3 (8 hrs) or treated with 100 ng/mL poly I:C/LyoVec for 12 hrs. Data are shown as mean ± standard deviation. Asterisks indicate p-values of ≤0.05. (**D**) Luciferase assay (expressed in relative luciferase activity) from HEK293 cells transfected with the indicated constructs and IFNβ promoted luciferase constructs for 24 hrs and then infected with CVB3 (1 PFU/cell) for 14 hrs. (**E**), IFNβ production as measured by ELISA from HEK293, HeLa, or Caco-2 cell culture supernatants infected with either CVB3 (3PFU/cell) or VSV (5PFU/cell) for the indicated times. Data are shown as the fold IFNβ induction compared to no virus (NoV) controls. Data in (D) and (E) shown as mean ± standard deviation. Asterisks indicate p-values ≤0.05.
doi:10.1371/journal.ppat.1001311.g001

MAVS (D429E, [24]) had no effect on CVB3-induced MAVS cleavage (Supplemental Figure S2C), indicating a caspase-independent mechanism of action.

Another common pathway upstream of IRF3 activation is the engagement of TLR3 by viral dsRNA, which is produced as a replication intermediate during viral infection. As we observed cleavage of MAVS in CVB3-infected cells, we sought to determine if CVB3 might also target TRIF, the specific adaptor molecule downstream of TLR3, to repress IRF3 activation. Similar to our findings with MAVS, we found that TRIF expression was significantly reduced in HeLa cells infected with CVB3 (Figure 2F). Although TRIF can be cleaved during apoptosis [23,24], we found that z-VAD-FMK and MG132 had little effect at antagonizing the CVB3-mediated reduction in TRIF expression (Figure 2F), consistent with our findings with MAVS (Figure 2A). The kinetics of TRIF cleavage also paralleled that of MAVS as we observed a marked reduction in TRIF levels by 3 hrs p.i. (Figure 2G), a time prior to the induction of caspase-3 cleavage (Figure 2B). Ectopically expressed CFP-fused TRIF was also significantly decreased in cells infected with CVB3 and coincided with the appearance of several cleavage fragments (Figure 2H).

We next investigated whether cleavage of MAVS and TRIF occurred in cells infected with other enteroviruses including echovirus 7 (E7) and enterovirus 71 (EV71). Infection of HeLa cells with both E7 and EV71 led to the significant reduction of MAVS and TRIF expression, which corresponded with the appearance of the newly replicated viral protein VP1 (Supplemental Figure S3A). However, in contrast to our findings with CVB3 (Figure 2A), we did not observe the appearance of any significant cleavage fragments in either E7 or EV71-infected cells. This may indicate that the cleavage fragments are short-lived in E7 or EV71-infected cells or that cleavage occurs at different residues within the molecule that alter antibody binding. These results may indicate that members of the enterovirus family target MAVS and TRIF to evade host immunity, but further studies are required to definitively show which members of the enterovirus family utilize this mechanism.

CVB3 infections are commonly associated with virus-induced heart disease in adults and children and have been detected in approximately 20-25% of patients with dilated cardiomyopathy and myocarditis [13,14,15,16]. To determine whether MAVS and TRIF are degraded *in vivo*, mice were infected with CVB3 and the hearts of infected animals were probed for MAVS and TRIF. In contrast to uninfected controls, there was an almost complete absence of both MAVS and TRIF in murine hearts infected with CVB3 (Supplemental Figure S3B). These data indicate that the cleavage of MAVS and TRIF may also occur during CVB3 infection *in vivo*.

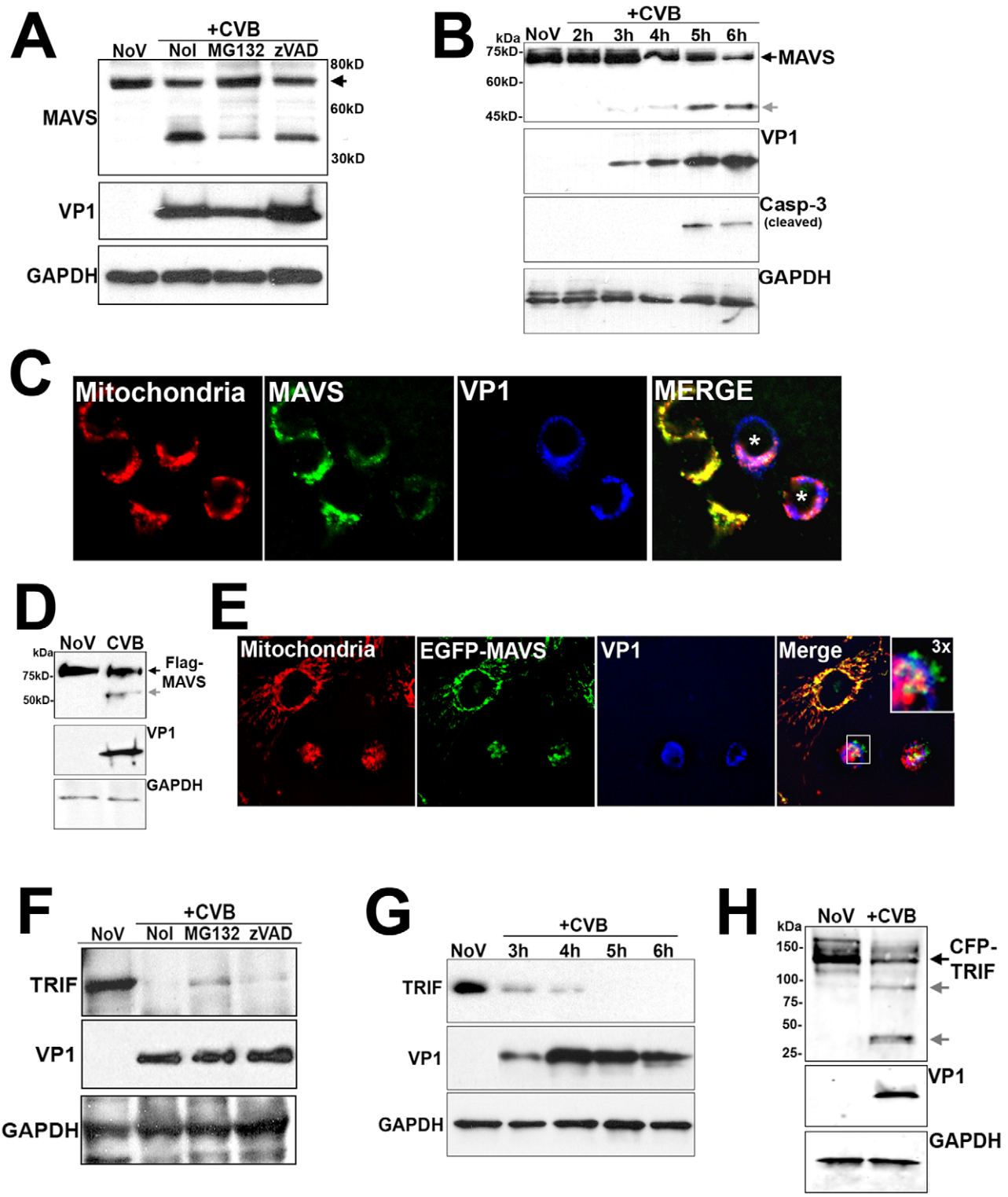

Figure 2. CVB3 infection induces MAVS and TRIF cleavage. (**A**) Western blot analysis for MAVS in HEK293 cells infected with CVB3 for 12 hrs in the absence (NoI) or presence of Z-VAD-FMK (zVAD) or MG132. (**B**) Time course of MAVS and caspase-3 cleavage in HEK293 cells infected with CVB3 for the indicated times. (**C**) HEK293 cells were infected with CVB3 for 8 hrs and fixed and stained for MAVS (green), mitochondria (red), and VP1 (blue). Asterisks denote infected cells expressing less MAVS than uninfected controls. (**D**, **E**) U2OS cells transfected with Flag-MAVS or EGFP-MAVS were infected with CVB3 (1 PFU/cell) for 7 hrs (D) or 12 hrs (E) and then lysed and immunoblotted with anti-Flag monoclonal antibody (D) or fixed and stained for mitochondria (red) and VP1 (blue) (E). In order to better visualize cleavage fragments in (D), CVB-infected cultures were transfected with 2 μg Flag-MAVS (in comparison to 1 μg in uninfected controls). (**F**) Western blot analysis for TRIF in HeLa cells infected with CVB3 for 8 hrs in the absence (NoI) or presence of z-VAD-FMK (zVAD) or MG132. (**G**) Time course of TRIF cleavage in HeLa cells infected with CVB3 (1 PFU/cell) for the indicated times. (**H**) Immunoblot analysis for overexpressed CFP-TRIF in HEK293 cells infected with CVB3 (1 PFU/cell) for 8 hrs. In (A), (D), and (H), grey arrows denote CVB3-induced cleavage fragments.
doi:10.1371/journal.ppat.1001311.g002

CVB3 3C^{pro} cleaves MAVS and TRIF

Enteroviruses encode specific proteases that are required for the processing of viral proteins and the establishment of replication, but which also cleave a variety of host cell molecules [29]. Because we observed the cleavage of MAVS in CVB3-infected cells, we investigated whether virally-encoded proteases might mediate this effect. We cotransfected HEK293 cells with N-terminal Flag-MAVS and various CVB3 viral proteins fused to EGFP. Of these proteins, we found that expression of the protease 3C^{pro} was sufficient to induce a significant reduction in MAVS expression (Figure 3A). In fact, in order to observe significant levels of full-length Flag-MAVS (or cleavage fragments) in EGFP-3C^{pro} co-transfected cells, cells had to be transfected with twice as much Flag-MAVS as vector control or other CVB3 viral proteins. The apparent lack of cleavage products in cells overexpressing proteases is a phenomenon that has also been observed for HCV-mediated cleavage of TRIF [11] and likely reflects the high efficiency of cleavage (which may result from protease overexpression) and that cleavage fragments are unstable and/or short-lived. For our subsequent studies, we transfected cells with equivalent amounts of MAVS cDNA to compare the level of full-length MAVS in control versus 3C^{pro}-transfected cells. The cleavage of MAVS required the cysteine protease activity of 3C^{pro}, as cotransfection of a catalytically inactive N-terminal EGFP-tagged 3C^{pro} mutant (C147A) [30] had no effect on MAVS expression (Figure 3B). In some cases, significant levels of GFP signal alone can be detected in EGFP-3C^{pro} WT transfected cells which is likely indicative of 3C^{pro} cleaving itself from the N-terminal EGFP tag.

To confirm that 3C^{pro} was directly cleaving MAVS, we incubated recombinant wild-type or C147A mutant 3C^{pro} with Flag-MAVS purified by Flag column affinity purification from overexpressing HEK293 cells. Whereas incubation with wild-type 3C^{pro} induced the appearance of a MAVS cleavage fragment as determined by Flag immunoblotting, the C147A mutant did not induce the appearance of a MAVS cleavage product (Figure 3C).

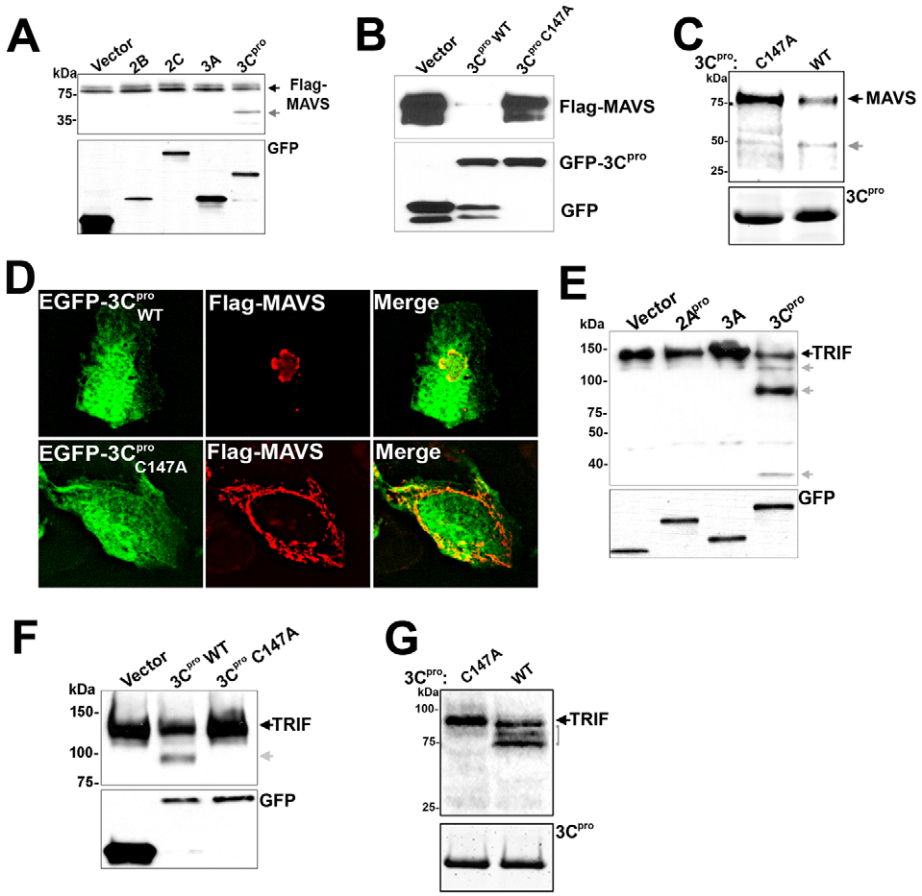

Figure 3. 3C^{pro} Cleaves MAVS and TRIF. (**A**) Immunoblot analysis for Flag-MAVS (top) and GFP (bottom) in HEK293 cells co-transfected with EGFP-2B, 2C, 3A, or 3C^{pro} and Flag-MAVS. In order to better visualize cleavage fragments, EGFP-3C^{pro} expressing cells were transfected with 2 μg Flag-MAVS (in comparison to 1 μg with other constructs). (**B**) HEK293 cells transfected with Flag-MAVS and control (EGFP-C2), EGFP-3Cpro wild-type or C147A were lysed and subjected to immunoblotting for MAVS and GFP. (**C**) 3C^{pro} cleaves MAVS *in vitro*. Recombinant wild-type or C147A mutant SUMO-3C^{pro} (10 μg) was incubated with column purified Flag-MAVS (0.1 μg) for 8 hrs at 37°C, fractionated by SDS-PAGE, and immunoblotted with anti-Flag monoclonal antibody (top) or commassie stained (bottom). (**D**) U2OS cells were transfected with EGFP-3C^{pro} wild-type (WT) or the C147A mutant and Flag-MAVS and immunofluorescence microscopy performed for MAVS (in red). (**E**) Immunoblot analysis of HEK293 cells transfected with CFP-TRIF and either vector control, EGFP-2A^{pro}, 3A EGFP-3C^{pro} and lysates immunoblotted for TRIF (top) or GFP (bottom). Grey arrows denote 3C^{pro}-induced cleavage products. (**F**) Lysates of HEK293 cells transfected with CFP-TRIF and vector, wild-type (WT), or C147A mutant EGFP-3C^{pro} were immunoblotted with anti- TRIF antibody (top) or anti-GFP (bottom) antibodies. Grey arrow denotes 3C^{pro}-induced cleavage product. (**G**) 3C^{pro} cleaves TRIF *in vitro*. Recombinant wild-type or C147A mutant SUMO-3C^{pro} (10 μg) was incubated with column purified Flag-TRIF (0.1 μg) for 12 hrs at 37°C, fractionated by SDS-PAGE, and immunoblotted with anti-Flag monoclonal antibody (top) or commassie stained (bottom).
doi:10.1371/journal.ppat.1001311.g003

Moreover, whereas expression of wild-type EGFP-3C^{pro} induced the relocalization of MAVS as assessed by immunofluorescence microscopy, expression of EGFP-3C^{pro} C147A had no effect (Figure 3D).

Because we also observed cleavage of TRIF in CVB3-infected cells, we determined whether 3C^{pro} was responsible for its cleavage as well. We cotransfected HEK293 cells with TRIF and either EGFP-2A^{pro}, 3A, or -3C^{pro}. Expression of 3C^{pro}, but not 2A^{pro} or 3A, led to the cleavage of TRIF, demonstrated by a reduction in the expression of full-length TRIF and the appearance of several TRIF cleavage fragments (Figure 3E). 3C^{pro}-mediated cleavage of TRIF required the cysteine protease activity of 3C^{pro} as expression of 3C^{pro} C147A did not lead to TRIF cleavage (Figure 3F). We also confirmed that 3C^{pro} was directly cleaving TRIF by incubation of Flag-TRIF purified by Flag column affinity purification from overexpressing HEK293 cells with recombinant wild-type or C147A mutant 3C^{pro}. Similar to our findings with MAVS (Figure 3C), we found that only recombinant wild-type 3C^{pro} induced the appearance of TRIF cleavage fragments (Figure 3G). Note that the pattern of TRIF cleavage by *in vitro* proteolysis assay (Figure 3G) differs from our experiments with overexpressed 3C^{pro} in HEK293 cells (Figure 3E, 3F) due to the use of C-terminal CFP- versus N-terminal Flag-tagged TRIF between experiments. Taken together, our data show that 3C^{pro} directly cleaves both MAVS and TRIF.

3C^{pro} disrupts MAVS and TRIF type I IFN and apoptotic signaling

To assess whether expression of 3C^{pro} abrogated MAVS-dependent signaling, we transfected HEK293 cells with wild-type or C147A EGFP-3C^{pro} or vector control, with a luciferase reporter fused to the IFNβ promoter region (p-125-Luc), and with either Flag-MAVS or the caspase activation and recruitment domains (CARDs) of MDA5 or RIG-I. Expression of the CARDs of MDA5 and RIG-I alone results in the constitutive activation of type I IFN signaling even in the absence of stimulus [31]. We found that whereas there was pronounced induction of IFNβ activity in cells expressing vector alone or EGFP-3C^{pro} C147A, expression of wild-type EGFP-3C^{pro} led to a significant reduction in promoter activity (Figure 4A).

We next determined whether 3C^{pro} attenuated TRIF-mediated signaling. TRIF is involved in the activation of IRF3 and IFNβ induction downstream of dsRNA-TLR3 engagement. While the expression of TRIF and vector control enhanced IFNβ promoter activity, expression of TRIF in combination with 3C^{pro} significantly impaired IFNβ promoter activity (Figure 4B). We found that 3C^{pro}-mediated inhibition of IFNβ signaling was indeed occurring upstream of IRF3 activation as coexpression of wild-type 3C^{pro} and IRF3 had no effect on IRF3-mediated activation of IFNβ promoter activity (Supplemental Figure S4A). Furthermore, we found that expression of wild-type, but not C147A 3C^{pro} reduced IFNβ activation in response to infection with VSV (Supplemental Figure S4B).

In addition to their roles in type I IFN signaling, ectopic expression of MAVS [32] and TRIF [33] potently stimulate intrinsic apoptotic machinery to induce cell death. We found that expression of MAVS or TRIF induced pronounced apoptosis as demonstrated by enhanced Annexin V binding [which identifies the externalization of phosphatidylserine in cells undergoing apoptosis] (Figure 4C, 4D). In contrast, expression of MAVS or TRIF in the presence of 3C^{pro} potently reduced apoptosis (Figure 4C, 4D). Taken together, these data show that 3C^{pro} represses both the apoptotic and type I IFN signaling mediated by MAVS and TRIF.

3C^{pro} cleaves MAVS within the proline rich region

3Cpro preferentially cleaves glutamine-glycine (Q-G) bonds in both the viral polyprotein and cellular targets, but may also exhibit

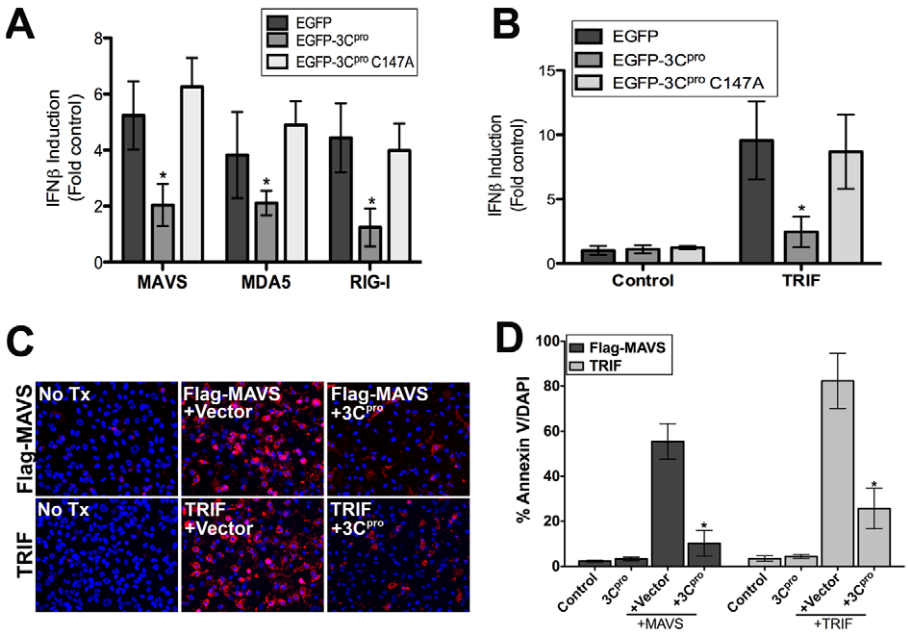

Figure 4. 3C^{pro} abrogates MAVS and TRIF Type I IFN and apoptotic signaling. (**A**,**B**) Luciferase assay (expressed as fold IFNβ induction versus vector controls) from HEK293 cells transfected with vector, EGFP-3C^{pro} wild-type or C147A mutants, the CARDs of MAVS, MDA5, or RIG-I, and a IFNβ promoted luciferase construct. Data are shown as mean ± standard deviation. Asterisks indicate p-values ≤0.05 (**C**) Representative images of either untransfected (No Tx) U2OS cells or cells transfected with Flag-MAVS (top row) or TRIF (bottom row) and either vector alone (+Vector) or wild-type (WT) EGFP-3C^{pro}. Cells were stained with Alexa Fluor 594-conjugated Annexin V 48 hrs post-transfection. Blue, DAPI-stained nuclei. (**D**) Quantification of the extent of apoptosis (shown as the percent of Annexin V positive cells/DAPI) in cells from (C). Asterisks indicate p-values ≤0.05.
doi:10.1371/journal.ppat.1001311.g004

proteolytic activity against glutamine-alanine (Q-A) bonds, amongst others [29]. In order to identify the residue(s) within MAVS cleaved by $3C^{pro}$, we constructed a panel of site directed mutants within MAVS at residues that may serve as $3C^{pro}$ cleavage sites (Q148, Q211, and E480) (Figure 5A). Of these mutants, only one (Q148A) was resistant to $3C^{pro}$-mediated cleavage in HEK293 cells and by *in vitro* protease assay (Figure 5B). Moreover, whereas wild-type Flag-MAVS was relocalized from the mitochondrial membrane upon expression of EGFP-$3C^{pro}$, the Q148A Flag-MAVS mutant retained its mitochondrial localization (Figure 5C). The $3C^{pro}$ cleavage site within MAVS (Q148) is located in the proline rich region, which mediates its interaction with a number of signaling molecules including TRAF2 [4], TRAF3 [34], TRAF6 [4], RIP1 [2], and FADD [2].

We next determined whether the Q148A mutant of MAVS was resistant to $3C^{pro}$-mediated abatement of MAVS signaling. We found that whereas there was a pronounced reduction in IFNβ activity in cells expressing wild-type Flag-MAVS and EGFP-$3C^{pro}$, there was no effect of EGFP-$3C^{pro}$ expression on IFNβ signaling in cells transfected with Q148A Flag-MAVS (Figure 5D, Supplemental Figure S2D). These data show that CVB3 $3C^{pro}$ cleaves MAVS at Q148 to suppress MAVS signaling.

$3C^{pro}$-induced MAVS cleavage fragments exhibit reduced function

MAVS requires an intact CARD and localization to the mitochondrial membrane (via a C-terminal transmembrane domain) to remain functionally active [5]. Because we found that $3C^{pro}$ cleaved MAVS at a specific residue (Q148) within the proline rich region, we next determined whether either of the possible $3C^{pro}$-induced cleavage fragments of MAVS would remain active. To that end, we constructed EGFP-fused constructs expressing wild-type MAVS, the N-terminal (residues 1-148), or C-terminal (residues 149-540) fragments of MAVS that would result from $3C^{pro}$ cleavage (Figure 5F). We found that the N-terminal fragment of MAVS (1-148) no longer localized to the mitochondrial membrane (Figure 5G) and induced NFκB or IFNβ signaling significantly less that full-length MAVS (Figure 5H). Whereas the C-terminal fragment of MAVS (149-540) retained its mitochondrial localization (Figure 5G), it also exhibited significantly less NFκB and IFNβ activation in comparison to full-length MAVS (Figure 5H). These data indicate that $3C^{pro}$-mediated cleavage of MAVS likely inactivates MAVS-mediated downstream signaling by directly cleaving a residue that separates the CARD and transmembrane regions.

$3C^{pro}$ localizes to the TRIF signalosome and interacts with the C-terminus of TRIF

Overexpressed TRIF forms multimers and localizes to punctate cytoplasmic structures referred to as the TRIF 'signalosome' [35]. Downstream components of TRIF signaling localize to signalosomes as a mechanism to stimulate TRIF signaling [35,36]. We found that EGFP-$3C^{pro}$ and EGFP-$3C^{pro}$ C147A were recruited to TRIF signalosomes when co-expressed with TRIF (Figure 6A). This recruitment was specific for $3C^{pro}$ as we did not observe the recruitment of either EGFP-$2A^{pro}$ (not shown) or EGFP-3A (Supplemental Figure S5) to TRIF signalosomes. Although TLR3 (and presumably TRIF) can localize to endosomal membranes [37], we did not observe any colocalization of overexpressed TRIF with markers of both early and late endosomes (Supplemental Figure S6).

Because we observed the relocalization of $3C^{pro}$ to the signalosome complex, we next determined whether $3C^{pro}$ and TRIF interact within this specialized complex. HEK293 cells were transfected with TRIF and either vector (EGFP alone), EGFP-$3C^{pro}$ wild-type, or EGFP-$3C^{pro}$ C147A and co-immunoprecipitation studies were performed. We found that whereas EGFP-$3C^{pro}$ C147A and TRIF co-immunoprecipitated, wild-type EGFP-$3C^{pro}$ and TRIF did not (Figure 6B). These findings indicate that $3C^{pro}$ forms an interaction with TRIF that is likely abolished upon $3C^{pro}$-mediated cleavage.

TRIF contains a proline-rich N-terminal region, a Toll/Interleukin-1 receptor (TIR) domain, and a C-terminal region. To determine which TRIF domain is responsible for interacting with $3C^{pro}$ and recruiting it to the signalosome, we constructed N-terminal (NT, 1–359aa), C-terminal (CT, 360–712aa), and TIR (390–460aa) domain expression constructs of TRIF containing a HA-tag at the N-terminus and a Flag-tag at the C-terminus (Figure 6C). We then coexpressed these constructs with wild-type and C147A versions of $3C^{pro}$ and performed fluorescence microscopy and immunoprecipitation analysis. We found that $3C^{pro}$ C147A specifically interacted with the C-terminal domain of TRIF, but not the N-terminus (Figure 6D). However, the TIR domain did not mediate the interaction between TRIF and $3C^{pro}$ as we observed no co-immunoprecipitation between HA-TIR-Flag and $3C^{pro}$ (not shown).

Previous studies have shown that expression of the C-terminus of TRIF is required for the formation of the TRIF signalosome [36]. We found that expression of HA-CT-Flag was sufficient to induce the relocalization of $3C^{pro}$ C147A to signalosomes (Figure 6E). In contrast, $3C^{pro}$ C147A did not localize with either HA-NT-Flag or HA-TIR-Flag (Figure 6E). The formation of tubule-like structures induced by the expression of the TRIF TIR is consistent with previous work by others [36]. Taken together, these data indicate that $3C^{pro}$ interacts with the C-terminus of TRIF that is sufficient for its recruitment into the TRIF signalosome.

$3C^{pro}$ cleaves the N- and C-terminal regions of TRIF

We did not observe any interaction between wild-type $3C^{pro}$ and either full-length or C-terminal TRIF (Figure 6D and 6E) suggesting that the interaction between TRIF and $3C^{pro}$ is diminished following cleavage. Interestingly, we observed the appearance of cleavage fragments of both HA-NT-Flag and HA-CT-Flag when coexpressed with wild-type $3C^{pro}$ (Figure 6D). To further define the extent of $3C^{pro}$-mediated proteolysis of the N- and C-terminal regions of TRIF, we coexpressed dually HA- and Flag-tagged constructs of TRIF (described in Figure 6C) and wild-type or C147A EGFP-$3C^{pro}$ and subjected lysates to dual-color (700 nm and 800 nm) immunoblot analysis using a LI-COR Odyssey infrared imaging system and antibodies specific for HA and Flag. This technique could therefore allow for the detection of a variety of TRIF cleavage fragments simultaneously. We found that expression of wild-type $3C^{pro}$ (but not the C147A mutant) induced the cleavage of both the N- and C-termini of TRIF (Figure 7A). In contrast, we observed no cleavage of the TIR domain (Figure 7A). Additionally, our data indicate that the C-terminus of TRIF is cleaved more abundantly than the N-terminus as we observed a marked decrease in the expression of full-length HA-CT-Flag and the appearance of several HA- or Flag-tag-positive cleavage products induced by $3C^{pro}$ overexpression (Figure 7A).

$3C^{pro}$ suppresses NFκB and Apoptotic signaling and via the C-terminus of TRIF

The N- and C-terminal regions of TRIF differ in their capacities to induce type I IFN and NFκB signaling—whereas overexpres-

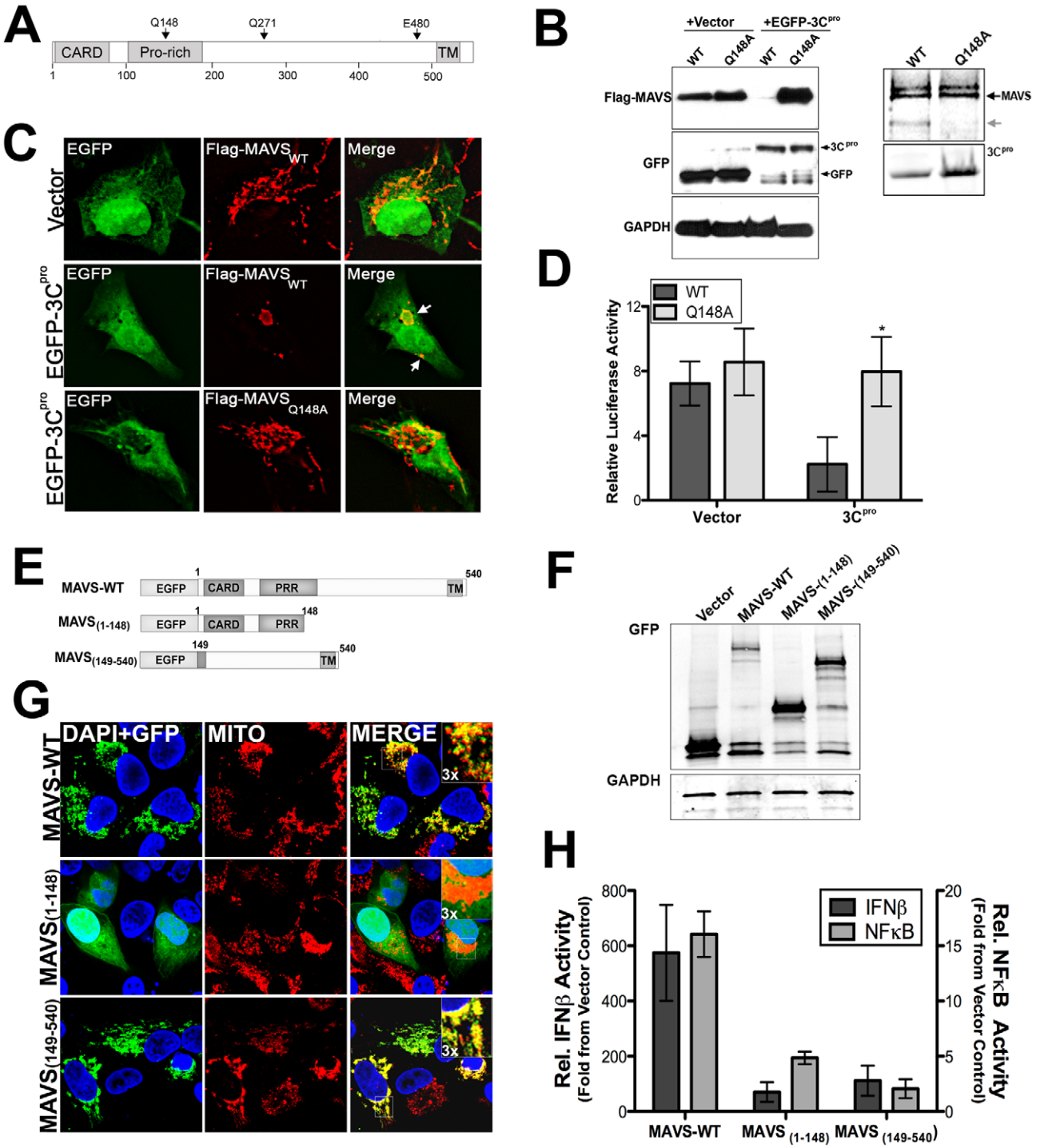

Figure 5. Q148 is the site of 3C^{pro}-mediated cleavage of MAVS. (**A**) Schematic of MAVS showing the locations of possible 3C^{pro} cleavage sites. (**B**) Left, Immunoblot analysis for overexpressed Flag-MAVS wild-type and the Q148A mutant in HEK293 cells cotransfected with either vector or EGFP-3C^{pro}. Right, recombinant wild-type SUMO-3C^{pro} (10 μg) was incubated with wild-type or Q148A column purified Flag-MAVS (0.1 μg) for 12 hrs at 37°C, fractionated by SDS-PAGE, and immunoblotted with anti-Flag monoclonal antibody (top) or commassie stained (bottom). (**C**) Immunofluorescence microscopy for Flag-MAVS wild-type (WT) of the Q148A mutant in U2OS cells co-transfected with EGFP-3C^{pro}. (**D**) Luciferase assay (expressed in relative luciferase activity) from HEK293 cells transfected with wild-type or Q148A Flag-MAVS and vector control or EGFP-3C^{pro} and IFNβ promoted luciferase constructs. Data are shown as mean ± standard deviation. Asterisks indicate p-values of ≤0.05. (**E**), Schematic of EGFP-fused MAVS constructs of 3C^{pro}-induced MAVS cleavage fragments. (**F**), Western blot analysis of HEK293 cells transfected with MAVS constructs depicted in (E). Lysates were immunoblotted with anti-monoclonal GFP antibody (top) or GAPDH as a loading controls (bottom). (**G**), Confocal microscopy of U2OS cells transfected with EGFP-fused MAVS 3C^{pro} cleavage fragments shown in (E). Cells were fixed and stained with anti-mitochondria monoclonal antibody (MITO) (red). Blue, DAPI stained nuclei. (**H**), Luciferase assay (expressed in relative luciferase activity) from HEK293 cells transfected with EGFP-fused MAVS 3C^{pro} cleavage fragments [from (E)] and NFκB or IFNβ promoted luciferase constructs. Data are shown as mean ± standard deviation. Asterisks indicate p-values ≤0.05.
doi:10.1371/journal.ppat.1001311.g005

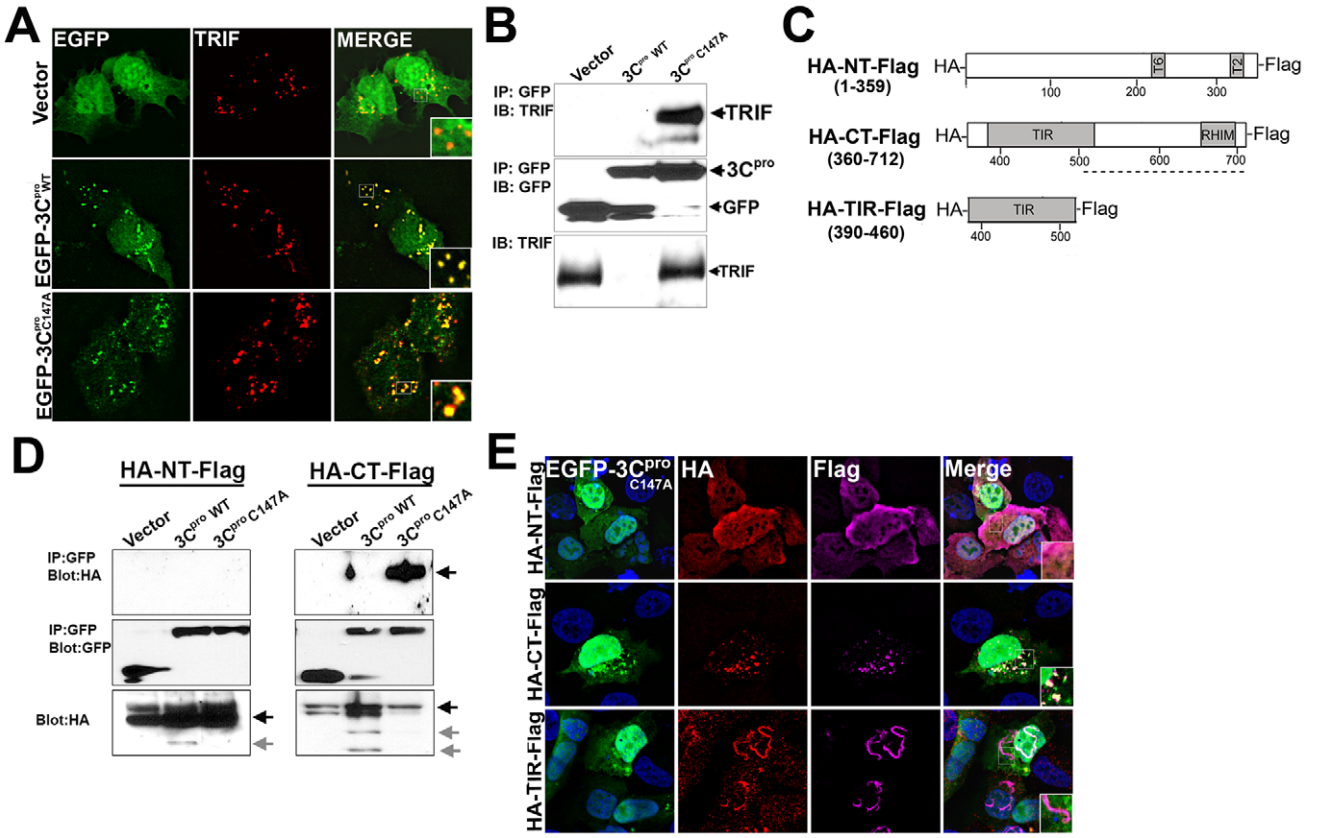

Figure 6. 3C^{pro} localizes to TRIF signalosomes and interacts with the C-terminal domain of TRIF. (**A**) Immunofluorescence microscopy for overexpressed TRIF (in red) in U2OS cells coexpressing vector control (EGFP-C2), or wild-type or C147A mutant EGFP-3C^{pro}. (**B**) HEK293 cells transfected with TRIF and vector, or wild-type or C147A mutant EGFP-3C^{pro} were lysed and subjected to immunoprecipitation with an anti-GFP monoclonal antibody. Immunoprecipitates were subjected to immunoblot analysis for TRIF and GFP. (**C**), Top, schematic of N-terminal HA-tagged and C-terminal Flag-tagged TRIF constructs. (**D**), HEK293 cells transfected with the indicated TRIF construct and either vector, wild-type or C147A mutant EGFP-3C^{pro} were lysed and subjected to immunoprecipitation with an anti-GFP monoclonal antibody. Immunoprecipitates were subjected to immunoblot analysis for HA and GFP. Arrows denote full-length (black) or cleaved (grey) TRIF. (**E**) Immunofluorescence microscopy for HA (in red), Flag (in purple), and EGFP and DAPI-stained nuclei in U2OS cells transfected with EGFP-3C^{pro} C147A and the indicated TRIF construct.
doi:10.1371/journal.ppat.1001311.g006

sion of the N-terminal region of TRIF activates both IFNβ and NFκB signaling, the C-terminal domain fails to activate IFNβ but potently induces NFκB activation [38,39]. Moreover, the C-terminus of TRIF is sufficient to induce apoptosis [33]. The RIP homotypic interaction motif (RHIM) at the C-terminus of TRIF is essential for both NFκB and apoptotic signaling [33,40]. Because we observed pronounced 3C^{pro}-mediated cleavage of the C-terminus of TRIF (Figure 7A), we investigated whether NFκB and apoptotic signaling mediated by the C-terminus of TRIF was abolished. We found that expression of wild-type 3C^{pro} potently abrogated NFκB and apoptotic signaling induced by expression of the C-terminus of TRIF (Figure 7B, 7C). These findings are consistent with those indicating that 3C^{pro} also inhibits full-length TRIF-mediated apoptotic signaling (Figure 4C, 4D).

3C^{pro} cleaves specific sites in the N- and C-terminal regions of TRIF

In order to identify the residue(s) within TRIF cleaved by 3C^{pro}, we constructed a panel of site directed mutants within the TRIF N- and C-terminal domains at residues that may serve as 3C^{pro} cleavage sites (Figure 7D). [We omitted any potential sites within the TRIF TIR domain as we did not observe 3C^{pro}-induced cleavage of this domain (Figure 7A)]. We found that a specific residue (Q190) within the N-terminal region of TRIF was targeted by 3C^{pro} as mutagenesis of this site abolished 3C^{pro}-induced cleavage (Figure 7E). Because several sites in the C-terminal domain of TRIF can serve as possible 3C^{pro} cleavage sites, and because these sites lie within close proximity to one another, we mutated these sites simultaneously. We found that simultaneous mutagenesis of four potential 3C^{pro} cleavage sites (Q653, Q659, Q671, and Q702) was sufficient to prevent 3C^{pro} cleavage (Figure 7F). These findings are consistent with our observation that the C-terminus of TRIF likely undergoes 3C^{pro} cleavage at several sites (Figure 7A).

3C^{pro}-induced TRIF cleavage fragments are nonfunctional in NFκB and apoptotic signaling

Because the N- and C-terminal domains of TRIF function in unique capacities to induce IRF3, NFκB, and apoptotic signaling, we next explored whether possible 3C^{pro} cleavage fragments of TRIF could remain functional in these pathways. We constructed EGFP-fused full-length TRIF and various possible cleavage fragments of TRIF (encoding residues 190-653, 190-671, or 190-702). We found that all three possible 3C^{pro} TRIF cleavage fragments maintained their capacity to activate type I IFN signaling (as assessed by luciferase assays for IFN- stimulated response element (ISRE), an IRF3-dependent promoter) (Figure 7G, 7H). In contrast, two of these fragments, 190–653

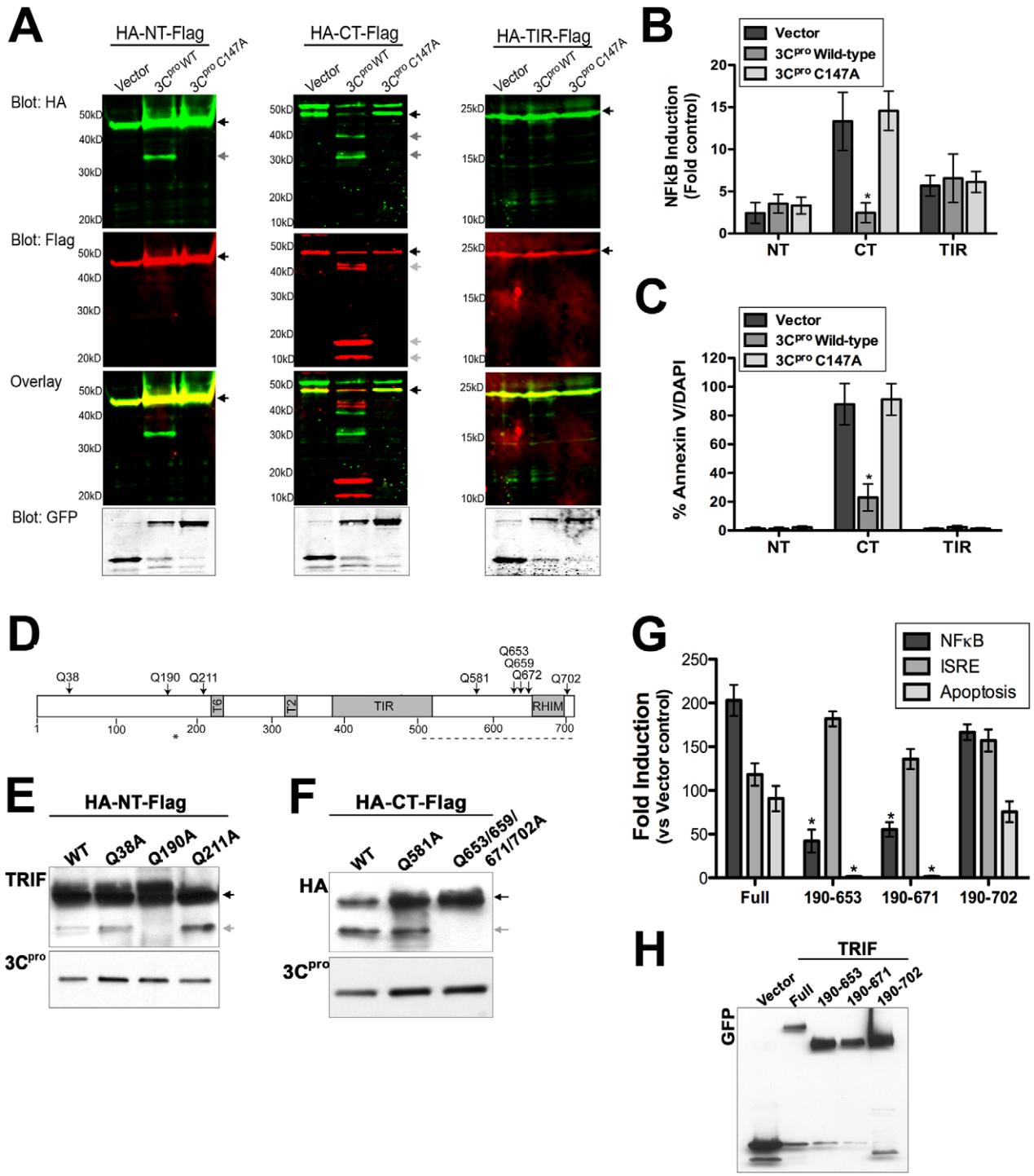

Figure 7. 3C^{pro} cleaves the N- and C-terminal domains of TRIF at specific sites. (**A**) Dual-color immunoblot analysis using a LI-COR Odyssey infrared imaging system and antibodies specific for HA (800 nm, green) and Flag (700 nm, red) in HEK293 cells transfected with vector, EGFP-3C^{pro} wild-type or C147A and the indicated TRIF plasmids (for schematic, see Figure 6C). Black arrows denote full-length TRIF and grey arrows denote cleavage fragments. An overlay of both channels is shown below (with yellow indicating overlapping signals). (**B**) Luciferase assay (expressed in relative luciferase activity) from HEK293 cells transfected with vector, wild-type or C147A EGFP-3C^{pro}, the indicated domains of TRIF, and a NFκB promoted luciferase construct. (**C**), Quantification of the extent of apoptosis (shown as the percent of Annexin V positive cells/DAPI) in HEK293 cells transfected with the indicated domains of TRIF and vector alone or wild-type of C147A mutant EGFP-3C^{pro}. (**D**) Schematic of TRIF showing the locations of possible 3C^{pro} cleavage sites. (**E**,**F**) Immunoblot analysis for wild-type or 3C^{pro}-resistant mutants of the N-terminal (HA-NT-Flag) (E) or C-terminal (HA-CT-Flag) (F) domains of TRIF from lysates of HEK293 cells transfected with the indicate constructs and EGFP-3C^{pro}. Immunblots were performed with anti-TRIF [NT-TRIF, (E)] or anti-HA [CT-TRIF, (F)]. (**G**). HEK293 cells were transfected with EGFP-fused full-length TRIF (Full) or possible possible 3C^{pro}-induced cleavage fragments of TRIF. Cells were either co-transfected NFκB and IFNβ promoted luciferase constructs and luciferase assays performed or the extent of apoptosis was measured by AnnexinV binding. Data are presented as fold-induction versus vector controls. (**H**), Lysates from cells described in (G) were harvested and immunoblotted with anti-GFP monoclonal antibody. Data in (B), (C), and (G) are shown as mean ± standard deviation. Asterisks indicate p-values ≤0.05.
doi:10.1371/journal.ppat.1001311.g007

and 190-671, lost their ability to activate NFκB or induce apoptotic signaling (Figure 7G, 7H). These data indicate that $3C^{pro}$-mediated cleavage of TRIF may primarily function to suppress TRIF-mediated NFκB and apoptotic signal propagation.

Discussion

The host innate immune response to viral infections often involves the activation of parallel PRR pathways that converge on the induction of type I IFNs and NFκB activation. Several viruses have evolved sophisticated mechanisms to evade the host innate immune response by directly interfering with the activation and/or downstream signaling events associated with PRR signal propagation. Here we show that the $3C^{pro}$ cysteine protease of CVB3 targets MAVS and TRIF, two key adaptor molecules in the innate immune response as a mechanism to suppress type I IFN and apoptotic signaling. By targeting these adaptors, CVB3 has evolved a strategy to suppress antiviral signal propagation through two powerful pathways—TLR3 and RIG-I/MDA5. $3C^{pro}$ cleaves MAVS at a specific site within its proline-rich region (at Q148) and suppresses MAVS-mediated induction of type I IFNs and apoptosis. Moreover, $3C^{pro}$ targets both the N- and C-terminal domains of TRIF to abrogate its type I IFN, NFκB, and apoptotic signaling capacities. Interestingly, we found that $3C^{pro}$ localized to TRIF signalosomes and interacted with the C-terminal domain of TRIF. Taken together, these data highlight the strategies used by CVB3 to evade the host innate immune response.

Many viruses target molecules upstream of IFN induction as a means to escape host immunity. Similar to our findings with CVB3 $3C^{pro}$, the $3C^{pro}$ of HAV directly cleaves MAVS to escape host immunity [8], but it is not known if HAV $3C^{pro}$ also cleaves TRIF. However, although HAV $3C^{pro}$ is responsible for mediating MAVS cleavage, the protease must be localized to the mitochondrial membrane via a transmembrane domain within the 3A viral protein in order to facilitate this event [8]. In contrast, CVB3 3A localizes to the ER membrane where it disrupts ER-Golgi vesicular trafficking [41,42] and is thus not targeted to the mitochondrial membrane. Our studies indicate that in contrast to HAV, CVB3 $3C^{pro}$ alone is sufficient to induce MAVS cleavage despite it not being localized to the mitochondrial membrane.

Although MAVS and TRIF are potent inducers of type I IFN signaling downstream of PRR activation, they have also been shown to induce apoptotic signaling–another powerful pathway used by host cells to suppress viral replication and progeny release. Enteroviruses are lytic viruses, and as such, possess no known mechanism for progeny release other than the destruction of the host cell membrane. Lytic viruses often develop efficient strategies to tightly regulate host cell death pathways in order to avoid killing the host cell prematurely (and terminating viral replication). CVB3 possesses anti-apoptotic strategies, which are mediated by the 2B and 2BC viral proteins [43,44]. In addition, it has been shown that $3C^{pro}$ targets the inhibitor of κBα as a means to stimulate apoptosis and suppress viral replication [45]. Our results show that $3C^{pro}$ may also serve in an anti-apoptotic capacity to suppress MAVS- and TRIF-mediated apoptotic signaling as a means to tightly regulate host cell apoptotic pathways. The pro-apoptotic signaling mediated by MAVS requires its localization to the mitochondrial membrane and the presence of intact CARDs, but not the presence of an intact proline-rich region [32]. Although $3C^{pro}$ cleaves MAVS within the proline-rich region (Q148, Figure 5B, 5C), this cleavage both induces the relocalization of MAVS from the mitochondrial membrane (Figure 5C) and inhibits MAVS signals (Figure 5D). Furthermore, $3C^{pro}$ cleavage fragments of MAVS are non-functional (Figure 5H). Thus, the loss of MAVS-induced apoptosis in CVB3 $3C^{pro}$-expressing cells is likely the result of both the relocalization of MAVS from the mitochondrial membrane and the inhibition of signaling via the CARD regions. Moreover, CVB3 $3C^{pro}$ targets the C-terminal region of TRIF, which has been shown to induce apoptosis via direct binding to receptor interacting protein 1 (RIP1) via its RIP homotypic interaction motif (RHIM) [33]. Specifically, we found that $3C^{pro}$ targeted several sites within the C-terminal domain of TRIF that could effectively remove the RHIM domain, a domain of TRIF known to be critically involved in NFκB and apoptotic signaling (Figure 7D, F). In support of this, we found that $3C^{pro}$ cleavage fragments were deficient in NFκB activation and apoptosis (Figure 7G). Taken together, these data indicate that $3C^{pro}$ suppresses MAVS and TRIF-induced apoptotic signals both by their direct cleavage and by their relocalization from either the mitochondria or signalosome, respectively.

The N- and C-terminal domains of TRIF serve disparate functions in the initiation of innate immune signaling. Whereas the N-terminus of TRIF activates type I IFN induction via the phosphorylation of IRF3, the C-terminal domain activates NFκB [38,39]. Interestingly, we found that $3C^{pro}$ cleaves both of these domains—likely as a mechanism to suppress global TRIF-generated signaling capacities. Upon ligand stimulation of TLR3 (or upon overexpression), activated TRIF forms signalosomes enriched in TRIF-associated signaling components including RIP1 and NFκB -activating kinase-associated protein 1 (NAP1) [35,36]. We found that $3C^{pro}$ localizes to the TRIF signalosome and that expression of the C-terminal domain of TRIF is sufficient to induce this localization (Figure 6A, 6E). Moreover, we found that $3C^{pro}$ interacts with the C-terminal domain of TRIF (Figure 6D). However, it remains unclear whether this interaction is direct or mediated via an adaptor molecule that also localizes to the signalosome. Additionally, we found that $3C^{pro}$ cleavage of the TRIF C-terminal domain leads to the disruption of TRIF signalosome formation (Supplemental Figure S7), which is required for the initiation of TRIF-mediated IRF3 and NFκB activation [36]. It is thus conceivable that $3C^{pro}$ attenuates TRIF-dependent signaling via direct cleavage, the degradation of the signalosome complex, and inhibition of the interactions between TRIF and downstream molecules that are required to propagate TRIF-dependent signals.

Although we found that $3C^{pro}$ cleavage fragments of TRIF were deficient in NFκB and apoptotic signaling, they retained their capacity to induce type I IFN signaling (Figure 7G). These data may indicate that the cleavage fragments of TRIF generated by $3C^{pro}$ cleavage are short-lived and do not accumulate within the cell. In support of this, we failed to identify TRIF cleavage products induced by CVB3 infection endogenously (Figure 2F, 2G). Alternatively, it remains possible that $3C^{pro}$-mediated disruption of TRIF signaling is not involved in the suppression of type I IFN signaling, but may instead target type II IFN signaling. Previous studies in TLR3 and TRIF deficient mouse models indicate that TLR3- and TRIF-mediated IFNγ production plays an important role in CVB3 infections *in vivo* [19]. Thus, TLR3 signaling via TRIF to induce type II IFNs may function as a parallel pathway to MDA5 and/or RIG-I-mediated induction of type I IFNs. In this scenario, $3C^{pro}$ would suppress the downstream propagation of both type I and II IFN signaling in order to evade host immunity.

Viruses often utilize elegant strategies to attenuate innate immune signaling in order to promote their propagation. Here we show that the $3C^{pro}$ cysteine protease of CVB3 (and likely other enteroviruses) attenuates innate immune signaling mediated by two potent antiviral adapter molecules, MAVS and TRIF. By

utilizing a variety of methods to abate MAVS and TRIF signaling, including both cleavage and retargeting from sites of signal propagation, $3C^{pro}$ can efficiently suppress both type I IFN and apoptotic signals aimed at clearing CVB3 infections. A better understanding of the mechanisms employed by enteroviruses to suppress host antiviral signaling could lead to the development of therapeutic interventions aimed at modulating viral pathogenesis.

Methods

Cells and viruses

Human embryonic kidney (HEK) 293, HeLa, and U2OS cells were cultured in DMEM-H supplemented with 10% FBS and penicillin/streptomycin. Human intestinal Caco-2 cells were cultured in MEM supplemented with 10% FBS and penicillin/streptomycin. Cells were screened for mycoplasma using a PCR-based mycoplasma test (Takara Bio USA) to prevent abnormalities in cellular morphology, transfection, and growth.

All experiments were performed with CVB3-RD, expanded as described [46]. Vesicular stomatitis virus (VSV) was kindly provided by Sara Cherry (University of Pennsylvania, Philadelphia, PA). Experiments measuring productive virus infection were performed with 0.1-1 plaque forming units (PFU)/cell for the indicated times. HeLa cells were infected with echovirus 7 and enterovirus 71 at a MOI = 0.1 for the indicated times.

Mouse infections were performed as described previously [47] and lysates kindly provided to us by Jeffrey M. Bergelson, Children's Hospital of Philadelphia.

Transfections

Plasmid transfections were performed using FuGENE 6 according to the manufacturer's protocol (Roche Applied Science). Following transfection, cells were plated as described above and used 48–72 hrs later.

Immunofluorescence microscopy

Cells cultured in collagen-coated chamber slides (LabTek, Nunc) were washed and fixed with either 4% paraformaldehyde or with ice-cold methanol. Cells were then permeabilized with 0.1% Triton X-100 in phosphate buffered saline (PBS) and incubated with the indicated primary antibodies for 1 hr at room temperature (RT). Following washing, cells were incubated with secondary antibodies for 30 min at room temperature, washed, and mounted with Vectashield (Vector Laboratories) containing 4′,6-diamidino-2-phenylindole (DAPI). For detection of apoptosis, cells were washed in cold PBS and incubated with Alexa-Fluor-488 conjugated-annexin V and propidium iodide for 15 min at room temperature. Cells were then washed, fixed in 4% paraformaldehyde, and images captured as described below. Images were captured using an Olympus IX81 inverted microscope equipped with a motorized $\mathcal{Z}$-axis drive. Images were generated by multiple-section stacking (0.2 mm stacks) and deconvolved using a calculated point-spread function (Slidebook 5.0). Confocal microscopy was performed with a FV1000 confocal laser scanning microscope (Olympus).

Antibodies

Rabbit polyclonal and mouse monoclonal antibodies directed against GFP (FL, B-2), GAPDH, HA (Y-11, F-7) and IRF3 (FL-425) were purchased from Santa Cruz Biotechnology. Mouse monoclonal anti-Flag (M2) was purchased from Sigma. Rabbit polyclonal antibodies to TRIF and MAVS (human and rodent specific) were purchased from Cell Signaling Technologies or Bethyl Laboratories, respectively. Mouse anti-enterovirus VP1 (Ncl-Entero) was obtained from Novocastra Laboratories (Newcastle upon Tyne, United Kingdom). Mitochondria antibody [MTC02] was purchased from Abcam. Mouse anti-enterovirus 71 antibody was purchased from Millipore. Alexa Fluor-conjugated secondary antibodies were purchased from Invitrogen.

Plasmids

Flag-MDA5, Flag-MAVS, and Flag-TRIF plasmids were kindly provided by Tianyi Wang (University of Pittsburgh). pUNO2-hTRIF was purchased from Invivogen. EGFP-$2A^{pro}$ 2B, 2C, 3A and -$3C^{pro}$ were constructed by amplification from CVB33 cDNA (kindly provided by Jeffrey Bergelson, Children's Hospital of Philadelphia) and cloned into the NT-GFP TOPO fusion vector (Invitrogen) following PCR amplification. EGFP-fusion constructs expressing cleavage fragments of MAVS and TRIF were generated by PCR amplification from Flag-MAVS or pUNO2-TRIF and cloned into the NT-GFP TOPO fusion vector (Invitrogen). CFP-TRIF was purchased from Addgene (plasmid 13644). Dual HA- and Flag-tagged TRIF constructs were generated by amplification of TRIF cDNA with primers encoding a N-terminal HA or C-terminal Flag tags and cloned into the XhoI and EcoRI sites of pcDNA3.1(+). Mutagenesis of $3C^{pro}$, MAVS and TRIF constructs were performed using Quickchange mutagenesis kit following the manufacturer's protocol (Stratagene). Primer sequences are available upon request.

Immunoblots and immunoprecipitations

Cell lysates were prepared with RIPA buffer (50 mM Tris-HCl [pH 7.4]; 1% NP-40; 0.25% sodium deoxycholate; 150 mM NaCl; 1 mM EDTA; 1 mM phenylmethanesulfonyl fluoride; 1 mg/ml aprotinin, leupeptin, and pepstatin; 1 mM sodium orthovanadate), and insoluble material was cleared by centrifugation at 700×g for 5 min at 4°C. Lysates (30-50 μg) were loaded onto 4–20% Tris-HCl gels (Bio-Rad, Hercules, CA) and transferred to polyvinylidene difluoride membranes. Membranes were blocked in 5% nonfat dry milk or 3% bovine serum albumin, probed with the indicated antibodies, and developed with horseradish peroxidase-conjugated secondary antibodies (Santa Cruz Biotechology), and SuperSignal West Pico or West Dura chemiluminescent substrates (Pierce Biotechnology).

Immunoblots in isolated mouse hearts and dually HA- and Flag-tagged TRIF constructs were conducted using an Odyssey Infrared Imaging System (LI-COR Biosciences). Tissue homogenized in lysis buffer (100 μg) or whole-cell lysates from transfected HEK293 cells (30 μg) were loaded onto 4–20% Tris-HCl gels, separated electrophoretically, and transferred to nitrocellulose membranes. Membranes were blocked in Odyssey Blocking buffer and then incubated with the appropriate antibodies overnight at 4°C in Odyssey Blocking buffer. Following washing, membranes were incubated with anti-rabbit or anti-mouse antibodies conjugated to IRDye 680 or 800CW and visualized with the Odyssey Infrared Imaging System according to the manufacturer's instructions.

For immunoprecipitations, HEK293 cells transiently transfected with the indicated plasmids were lysed with EBC buffer (50 mM Tris [pH 8.0], 120 mM NaCl, 0.5% Nonidet P-40, 1 mm phenylmethylsulfonyl fluoride, 0.5 μg/ml leupeptin, and 0.5 μg/ml pepstatin). Insoluble material was cleared by centrifugation. Lysates were incubated with the indicated antibodies in EBC buffer for 1 hr at 4°C followed by the addition of Sepharose G beads for an additional 1 hr at 4°C. After centrifugation, the beads were washed in NETN buffer (150 mm NaCl, 1 mm EDTA, 50 mm Tris-HCl (pH 7.8), 1% Nonidet P-40, 1 mm phenylmethylsulfonyl fluoride, 0.5 μg/ml leupeptin, and 0.5 μg/ml

pepstatin), then heated at 95°C for 10 min in Laemmli sample buffer. Following a brief centrifugation, the supernatant was immunblotted with the indicated antibodies as described above.

Expression and purification of recombinant proteins

Bacterial expression vectors encoding wild-type or C147A $3C^{pro}$ were constructed in pET-SUMO (which encodes a linear fusion consisting of an N-terminal 6xHis tag for affinity purification followed by SUMO) following PCR amplification according to the manufacturers protocol (Invitrogen). pET-SUMO-$3C^{pro}$ constructs were expressed in bacteria and purified by metal chelation resin columns (Qiagen). The resulting 6xHis-SUMO $3C^{pro}$ fusion proteins were treated with SUMO protease to create untagged proteins as per the manufacturer's instructions (Invitrogen) and then dialyzed.

For purification of MAVS and TRIF, 10 cm dishes of HEK2393 cells were transfected with Flag-MAVS or Flag-TRIF and lysed 48 hrs post-transfection. Lysates were purified over anti-Flag affinity gel columns, washed several times, and protein eluted by competition with five washes of 3x Flag peptide using the Flag M purification kit for mammalian expression systems (Sigma-Aldrich). Eluted protein was quantified by BCA protein assay and verified for purity by SDS-PAGE and immunoblot analysis.

Reporter gene assay

Activation of the NFκB and IFNβ promoter was measured by reporter assay. Cells were transfected in 24-well plates with p-125 luc (IFNβ) or NFκB reporter plasmid together with the indicated plasmids. Luciferase activity was measured by the Dual-Luciferase assay kit (Promega). All experiments were performed in triplicate and conducted a minimum of three times.

ELISA

To measure IFNβ production, the indicated cells were infected with either CVB or VSV and samples of culture supernatant removed at the indicated times. IFNβ levels in culture supernatant were determined by IFNβ ELISA according to the manufacturer's instructions (PBL Biomedical Laboratories).

Isolation of nuclear extracts

Nuclear extracts were prepared from HEK293 cells after infection with CVB3 for 12 hr. Cells were washed in ice-cold PBS and isolated by incubation in 10 mM EDTA for 10 min. Cells were pelleted at 1000×g for 5 min, washed in ice-cold PBS, and incubated with buffer A (10 mM HEPES [pH 7.9], 1.5 mM MgCl2, 10 mM KCl, 0.5 mM DTT, 0.5 mM PMSF, and 0.1% NP-40). The pellets were then resuspended in buffer B (20 mM HEPES [pH 7.9], 25% glycerol, 0.42 M NaCl, 1.5 mM MgCl2, 0.2 mM EDTA, 0.5 mM DTT, 0.5 mM PMSF, 5-μg/ml leupeptin, 5-μg/ml pepstatin, 5-μg/ml aprotinin). Samples were incubated on ice for 15 min before being centrifuged at 10,000×g. Nuclear extract supernatants were diluted with buffer C (20 mM HEPES [pH 7.9], 20% glycerol, 0.2 mM EDTA, 50 mM KCl, 0.5 mM DTT, 0.5 mM PMSF).

Statistical analysis

Data are presented as mean ± standard deviation. One-way analysis of variance (ANOVA) and Bonferroni's correction for multiple comparisons were used to determine statistical significance ($p<0.05$).

Gene IDs

(numbers were taken from GenBank at Pubmed): mitochondrial antiviral signaling protein (MAVS) 57506; Toll/IL-1 receptor domain-containing adaptor inducing interferon-beta (TRIF) 148022, toll-like receptor 3 (TLR3) 7098; Retinoic acid-inducible gene-I (RIG-I) 23586; melanoma-differentiation-associated gene 5 (MDA5) 64135; interferon regulatory factor 3 (IRF3) 3661.

Supporting Information

Figure S1 CVB infection is sensitive to type I interferons. (A) Western blot analysis for VP1 in HeLa cells pretreated with medium alone (Con) or medium containing 100 U or 1000 U of purified IFNβ for 24 hrs and then infected with CVB (1PFU/cell) for 10 hrs. (B) As a control, similar studies were performed with VSV. Western blot analysis for VSV-G in HeLa cells pretreated with medium alone (Con) or medium containing 100 U or 1000 U of purified IFNβ for 24 hrs and then infected with VSV (5PFU/cell) for 10 hrs.
Found at: doi:10.1371/journal.ppat.1001311.s001 (0.13 MB TIF)

Figure S2 CVB, but not VSV, infection induces MAVS cleavage. (A) Western blot analysis for MAVS in lysates from HeLa cells infected with CVB for 10 hrs in the absence (NoI) or presence of Z-VAD-FMK (zVAD) or MG132. (B) Western blot analysis for MAVS in lysates from HEK293 cells infected with CVB or VSV for 12 hrs. (C),HEK293 cells with transfected with D429E Flag-MAVS (1 μg in no virus (NoV) controls or 2 μg in CVB-infeceted culures) and then infected with CVB (1PFU/cell for 12 hrs) 48 hrs following transfection. Lysates were harvested and immunoblotted for Flag, VP1, or GAPDH (as a loading control). (D), Lysates from Figure 5D were immunoblotted for Flag and GFP.
Found at: doi:10.1371/journal.ppat.1001311.s002 (0.36 MB TIF)

Figure S3 MAVS and TRIF are cleaved by other enteroviruses and are absent from the hearts of CVB-infected mice. (A) Immunoblot analysis for MAVS and TRIF in HeLa cells infected with echovirus 7 (E7) or enterovirus 71 (EV71) for the indicated times (0.1 PFU/cell). (B) Hearts of three mice infected by intraperitoneal injection with CVB for 7 days were removed, homogenized, and lysed. Lysates were subjected to immunblot analysis for MAVS and TRIF using an Odyssey Infrared Imaging System (immunoblots are shown as grey scale images).
Found at: doi:10.1371/journal.ppat.1001311.s003 (0.17 MB TIF)

Figure S4 3Cpro acts upstream of IRF3 and attenuates VSV-induced IFNβ activation. (A), HEK293 cells were transfected with an IFNβ-luciferase construct and IRF3 either with or without 3Cpro. Lysates were harvested 48 hrs post-transfection and luciferase activity measured. (B), HEK293 cells were transfected with an IFNβ-luciferase construct and either vector control, or wild-type of C147A 3Cpro. 48 hrs post-transfections, cells were infected with VSV for 12 hrs, lysates collected and and luciferase activity measured.
Found at: doi:10.1371/journal.ppat.1001311.s004 (0.21 MB TIF)

Figure S5 CVB 3A does not localize to the TRIF signalosome. Immunofluoescence microscopy of U2OS cells transfected with EGFP-3A and TRIF (red).
Found at: doi:10.1371/journal.ppat.1001311.s005 (0.25 MB TIF)

Figure S6 TRIF does not localize to endosomes. U2OS cells transfected with TRIF were stained for early endosome antigen-1 (EEA1), the lysosomal marker LAMP2, or Alexa Fluor 488-conjugated transferrin (TRANS).
Found at: doi:10.1371/journal.ppat.1001311.s006 (1.72 MB TIF)

Figure S7 3Cpro inhibits signalsome formation. Immunofluoescence microscopy of EGFP-3Cpro wild-type and HA-CT-Flag (HA, red) in transfected U2OS cells.
Found at: doi:10.1371/journal.ppat.1001311.s007 (0.38 MB TIF)

Acknowledgments

We are grateful to Jeffrey Bergelson and Nicole K. LeLay for providing us with lysates of CVB3-infected hearts. We thank Eckard Wimmer and Chunling Wang for helpful discussions and Jeff Bergelson and Fred Homa for careful review of the manuscript.

Author Contributions

Conceived and designed the experiments: AM CBC. Performed the experiments: AM SAM EDA NDS CBC. Analyzed the data: AM CBC. Contributed reagents/materials/analysis tools: NDS MSO TW. Wrote the paper: CBC.

References

1. O'Neill LA, Bowie AG (2007) The family of five: TIR-domain-containing adaptors in Toll-like receptor signalling. Nat Rev Immunol 7: 353–364.
2. Kawai T, Takahashi K, Sato S, Coban C, Kumar H, et al. (2005) IPS-1, an adaptor triggering RIG-I- and Mda5-mediated type I interferon induction. Nat Immunol 6: 981–988.
3. Meylan E, Curran J, Hofmann K, Moradpour D, Binder M, et al. (2005) Cardif is an adaptor protein in the RIG-I antiviral pathway and is targeted by hepatitis C virus. Nature 437: 1167–1172.
4. Xu LG, Wang YY, Han KJ, Li LY, Zhai Z, et al. (2005) VISA is an adapter protein required for virus-triggered IFN-beta signaling. Mol Cell 19: 727–740.
5. Seth RB, Sun L, Ea CK, Chen ZJ (2005) Identification and characterization of MAVS, a mitochondrial antiviral signaling protein that activates NF-kappaB and IRF 3. Cell 122: 669–682.
6. Dixit E, Boulant S, Zhang Y, Lee AS, Odendall C, et al. (2010) Peroxisomes are signaling platforms for antiviral innate immunity. Cell 141: 668–681.
7. Li XD, Sun L, Seth RB, Pineda G, Chen ZJ (2005) Hepatitis C virus protease NS3/4A cleaves mitochondrial antiviral signaling protein off the mitochondria to evade innate immunity. Proc Natl Acad Sci U S A 102: 17717–17722.
8. Yang Y, Liang Y, Qu L, Chen Z, Yi M, et al. (2007) Disruption of innate immunity due to mitochondrial targeting of a picornaviral protease precursor. Proc Natl Acad Sci U S A 104: 7253–7258.
9. Chen Z, Benureau Y, Rijnbrand R, Yi J, Wang T, et al. (2007) GB virus B disrupts RIG-I signaling by NS3/4A-mediated cleavage of the adaptor protein MAVS. J Virol 81: 964–976.
10. Drahos J, Racaniello VR (2009) Cleavage of IPS-1 in cells infected with human rhinovirus. J Virol 83: 11581–11587.
11. Li K, Foy E, Ferreon JC, Nakamura M, Ferreon AC, et al. (2005) Immune evasion by hepatitis C virus NS3/4A protease-mediated cleavage of the Toll-like receptor 3 adaptor protein TRIF. Proc Natl Acad Sci U S A 102: 2992–2997.
12. Morens D, Ma PM (1995) Human Enterovirus Infections; Rotbart HA, editor. Washington D.C., ed. Normal American Society for Microbiology.
13. Tracy S, Chapman NM, McManus BM, Pallansch MA, Beck MA, et al. (1990) A molecular and serologic evaluation of enteroviral involvement in human myocarditis. J Mol Cell Cardiol 22: 403–414.
14. Bowles NE, Richardson PJ, Olsen EG, Archard LC (1986) Detection of Coxsackie-B-virus-specific RNA sequences in myocardial biopsy samples from patients with myocarditis and dilated cardiomyopathy. Lancet 1: 1120–1123.
15. Martin AB, Webber S, Fricker FJ, Jaffe R, Demmler G, et al. (1994) Acute myocarditis. Rapid diagnosis by PCR in children. Circulation 90: 330–339.
16. Jin O, Sole MJ, Butany JW, Chia WK, McLaughlin PR, et al. (1990) Detection of enterovirus RNA in myocardial biopsies from patients with myocarditis and cardiomyopathy using gene amplification by polymerase chain reaction. Circulation 82: 8–16.
17. Wessely R, Klingel K, Knowlton KU, Kandolf R (2001) Cardioselective infection with coxsackievirus B3 requires intact type I interferon signaling: implications for mortality and early viral replication. Circulation 103: 756–761.
18. Deonarain R, Cerullo D, Fuse K, Liu PP, Fish EN (2004) Protective role for interferon-beta in coxsackievirus B3 infection. Circulation 110: 3540–3543.
19. Negishi H, Osawa T, Ogami K, Ouyang X, Sakaguchi S, et al. (2008) A critical link between Toll-like receptor 3 and type II interferon signaling pathways in antiviral innate immunity. Proc Natl Acad Sci U S A 105: 20446–20451.
20. Richer MJ, Lavallee DJ, Shanina I, Horwitz MS (2009) Toll-like receptor 3 signaling on macrophages is required for survival following coxsackievirus B4 infection. PLoS One 4: e4127.
21. Kong L, Sun L, Zhang H, Liu Q, Liu Y, et al. (2009) An essential role for RIG-I in toll-like receptor-stimulated phagocytosis. Cell Host Microbe 6: 150–161.
22. Gitlin L, Barchet W, Gilfillan S, Cella M, Beutler B, et al. (2006) Essential role of mda-5 in type I IFN responses to polyriboinosinic:polyribocytidylic acid and encephalomyocarditis picornavirus. Proc Natl Acad Sci U S A 103: 8459–8464.
23. Rebsamen M, Meylan E, Curran J, Tschopp J (2008) The antiviral adaptor proteins Cardif and Trif are processed and inactivated by caspases. Cell Death Differ 15: 1804–1811.
24. Scott I, Norris KL (2008) The mitochondrial antiviral signaling protein, MAVS, is cleaved during apoptosis. Biochem Biophys Res Commun 375: 101–106.
25. Huber SA, Budd RC, Rossner K, Newell MK (1999) Apoptosis in coxsackievirus B3-induced myocarditis and dilated cardiomyopathy. Ann N Y Acad Sci 887: 181–190.
26. Henke A, Launhardt H, Klement K, Stelzner A, Zell R, et al. (2000) Apoptosis in coxsackievirus B3-caused diseases: interaction between the capsid protein VP2 and the proapoptotic protein siva. J Virol 74: 4284–4290.
27. Luo H, Zhang J, Cheung C, Suarez A, McManus BM, et al. (2003) Proteasome inhibition reduces coxsackievirus B3 replication in murine cardiomyocytes. Am J Pathol 163: 381–385.
28. Neznanov N, Dragunsky EM, Chumakov KM, Neznanova L, Wek RC, et al. (2008) Different effect of proteasome inhibition on vesicular stomatitis virus and poliovirus replication. PLoS One 3: e1887.
29. Blom N, Hansen J, Blaas D, Brunak S (1996) Cleavage site analysis in picornaviral polyproteins: discovering cellular targets by neural networks. Protein Sci 5: 2203–2216.
30. Lee CC, Kuo CJ, Ko TP, Hsu MF, Tsui YC, et al. (2009) Structural basis of inhibition specificities of 3C and 3C-like proteases by zinc-coordinating and peptidomimetic compounds. J Biol Chem 284: 7646–7655.
31. Yoneyama M, Kikuchi M, Matsumoto K, Imaizumi T, Miyagishi M, et al. (2005) Shared and unique functions of the DExD/H-box helicases RIG-I, MDA5, and LGP2 in antiviral innate immunity. J Immunol 175: 2851–2858.
32. Lei Y, Moore CB, Liesman RM, O'Connor BP, Bergstralh DT, et al. (2009) MAVS-mediated apoptosis and its inhibition by viral proteins. PLoS One 4: e5466.
33. Kaiser WJ, Offermann MK (2005) Apoptosis induced by the toll-like receptor adaptor TRIF is dependent on its receptor interacting protein homotypic interaction motif. J Immunol 174: 4942–4952.
34. Saha SK, Pietras EM, He JQ, Kang JR, Liu SY, et al. (2006) Regulation of antiviral responses by a direct and specific interaction between TRAF3 and Cardif. EMBO J 25: 3257–3263.
35. Funami K, Sasai M, Ohba Y, Oshiumi H, Seya T, et al. (2007) Spatiotemporal mobilization of Toll/IL-1 receptor domain-containing adaptor molecule-1 in response to dsRNA. J Immunol 179: 6867–6872.
36. Funami K, Sasai M, Oshiumi H, Seya T, Matsumoto M (2008) Homo-oligomerization is essential for Toll/interleukin-1 receptor domain-containing adaptor molecule-1-mediated NF-kappaB and interferon regulatory factor-3 activation. J Biol Chem 283: 18283–18291.
37. Johnsen IB, Nguyen TT, Ringdal M, Tryggestad AM, Bakke O, et al. (2006) Toll-like receptor 3 associates with c-Src tyrosine kinase on endosomes to initiate antiviral signaling. EMBO J 25: 3335–3346.
38. Oshiumi H, Matsumoto M, Funami K, Akazawa T, Seya T (2003) TICAM-1, an adaptor molecule that participates in Toll-like receptor 3-mediated interferon-beta induction. Nat Immunol 4: 161–167.
39. Yamamoto M, Sato S, Mori K, Hoshino K, Takeuchi O, et al. (2002) Cutting edge: a novel Toll/IL-1 receptor domain-containing adapter that preferentially activates the IFN-beta promoter in the Toll-like receptor signaling. J Immunol 169: 6668–6672.
40. Meylan E, Burns K, Hofmann K, Blancheteau V, Martinon F, et al. (2004) RIP1 is an essential mediator of Toll-like receptor 3-induced NF-kappa B activation. Nat Immunol 5: 503–507.
41. Choe SS, Dodd DA, Kirkegaard K (2005) Inhibition of cellular protein secretion by picornaviral 3A proteins. Virology 337: 18–29.
42. Wessels E, Duijsings D, Lanke KH, van Dooren SH, Jackson CL, et al. (2006) Effects of picornavirus 3A Proteins on Protein Transport and GBF1-dependent COP-I recruitment. J Virol 80: 11852–11860.
43. Salako MA, Carter MJ, Kass GE (2006) Coxsackievirus protein 2BC blocks host cell apoptosis by inhibiting caspase-3. J Biol Chem 281: 16296–16304.
44. Campanella M, de Jong AS, Lanke KW, Melchers WJ, Willems PH, et al. (2004) The coxsackievirus 2B protein suppresses apoptotic host cell responses by manipulating intracellular Ca2+ homeostasis. J Biol Chem 279: 18440–18450.
45. Zaragoza C, Saura M, Padalko EY, Lopez-Rivera E, Lizarbe TR, et al. (2006) Viral protease cleavage of inhibitor of kappaBalpha triggers host cell apoptosis. Proc Natl Acad Sci U S A 103: 19051–19056.
46. Coyne CB, Bergelson JM (2006) Virus-induced Abl and Fyn kinase signals permit coxsackievirus entry through epithelial tight junctions. Cell 124: 119–131.
47. Kallewaard NL, Zhang L, Chen JW, Guttenberg M, Sanchez MD, et al. (2009) Tissue-specific deletion of the coxsackievirus and adenovirus receptor protects mice from virus-induced pancreatitis and myocarditis. Cell Host Microbe 6: 91–98.

nature immunology

The cytosolic nucleic acid sensor LRRFIP1 mediates the production of type I interferon via a β-catenin-dependent pathway

Pengyuan Yang[1,2], Huazhang An[1,2], Xingguang Liu[1], Mingyue Wen[1], Yuanyuan Zheng[1], Yaocheng Rui[1] & Xuetao Cao[1]

© 2010 Nature America, Inc. All rights reserved.

Intracellular nucleic acid sensors detect microbial RNA and DNA and trigger the production of type I interferon. However, the cytosolic nucleic acid–sensing system remains to be fully identified. Here we show that the cytosolic nucleic acid–binding protein LRRFIP1 contributed to the production of interferon-β (IFN-β) induced by vesicular stomatitis virus (VSV) and *Listeria monocytogenes* in macrophages. LRRFIP1 bound exogenous nucleic acids and increased the expression of IFN-β induced by both double-stranded RNA and double-stranded DNA. LRRFIP1 interacted with β-catenin and promoted the activation of β-catenin, which increased IFN-β expression by binding to the C-terminal domain of the transcription factor IRF3 and recruiting the acetyltransferase p300 to the IFN-β enhanceosome via IRF3. Therefore, LRRFIP1 and its downstream partner β-catenin constitute another coactivator pathway for IRF3-mediated production of type I interferon.

Type I interferons can be induced by many kinds of viruses and non-viral pathogens and are important in innate immune responses for the control of infection. Host pattern-recognition receptors (PRRs) recognize conserved components of invading microbes to mediate the production of type I interferon. Most extracellular bacteria induce such interferon production through membrane-associated Toll-like receptor (TLR) pathways. For example, Gram-negative bacteria lipopolysaccharide (LPS) is recognized by TLR4, which recruits the adaptor protein TRIF to activate the downstream kinases TBK1 and IKKε and, subsequently, the transcription factors NF-κB and IRF3 to initiate the transcription of genes encoding type I interferons[1,2].

Pathogen double-stranded RNA (dsRNA) is a potent activator of the innate immune response by inducing the production of type I interferon. Several PRR pathways in mammalian cells are responsible for sensing pathogen dsRNA. TLR3 was the first PRR identified as a sensor of viral dsRNA[3]. TLR3 recognizes dsRNA and mediates the production of type I interferon through a TRIF-dependent pathway. The cytosolic nucleic acid sensors RIG-I and Mda5 are the main PRRs that sense intracellular dsRNA[4,5]. RIG-I and Mda5 activate the expression of genes encoding type I interferons by a pathway dependent on the signaling adaptor MAVS (IPS-1)[6], which mediates this gene expression by activating IRF3 and NF-κB. In addition to recognizing single-stranded RNA (ssRNA) containing a 5′-triphosphate moiety[7], RIG-I also recognizes short dsRNA produced by RNA viruses such as vesicular stomatitis virus (VSV)[8]. In contrast, Mda5 recognizes long dsRNA produced by viruses such as encephalomyocarditis virus[8]. It remains to be determined whether there are other unknown PRRs involved in the sensing of intracellular dsRNA.

Cytosolic double-stranded DNA (dsDNA) is also a potent activator of innate immune responses in mammalian cells. Cytosolic dsDNA can be introduced into mammalian cells during infection by DNA viruses and intracellular bacteria. Detection of the cytosolic microbial DNA by host cells to induce the production of type I interferon is important for pathogen elimination. Thus, identifying DNA-sensing systems that can trigger the production of type I interferon has attracted much attention in recent years. So far, several cytosolic DNA sensors have been characterized through the use of synthetic dsDNA analogs such as CpG oligodeoxynucleotides, poly(dA:dT) (B-form DNA) and poly(dG:dC) (Z-form DNA). The first membrane-associated DNA sensor to be identified, TLR9, recognizes CpG DNA but mediates the production of type I interferon only in plasmacytoid dendritic cells[9]. Two cytosolic DNA sensors subsequently identified are DAI (ZBP1) and AIM2 (refs.10–14). However, DAI deficiency does not substantially impair the production of type I interferon induced by cytosolic B-form DNA in some kinds of primary cells of the immune system, which indicates the presence of additional DNA sensors[15,16]. Moreover, AIM2 binds dsDNA to induce IL-1β production through the inflammasome pathway without affecting the production of type I interferon[11–14,17,18]. Two studies have independently identified RNA polymerase III as an additional cytosolic sensor of B-form DNA for triggering the production of type I interferon[19–21]. Cytosolic RNA polymerase III can convert cytosolic AT-rich dsDNA into AU-rich dsRNA with a 5′-triphosphate moiety, which is then recognized by RIG-I to induce the production of interferon-β (IFN-β). However, this RNA polymerase III–dependent pathway does not sense

[1]National Key Laboratory of Medical Immunology and Institute of Immunology, Second Military Medical University, Shanghai, China. [2]These authors contributed equally to this work. Correspondence should be addressed to X.C. (caoxt@immunol.org) or H.A. (anhz@immunol.org).

Received 4 December 2009; accepted 9 April 2010; published online 9 May 2010; doi:10.1038/ni.1876

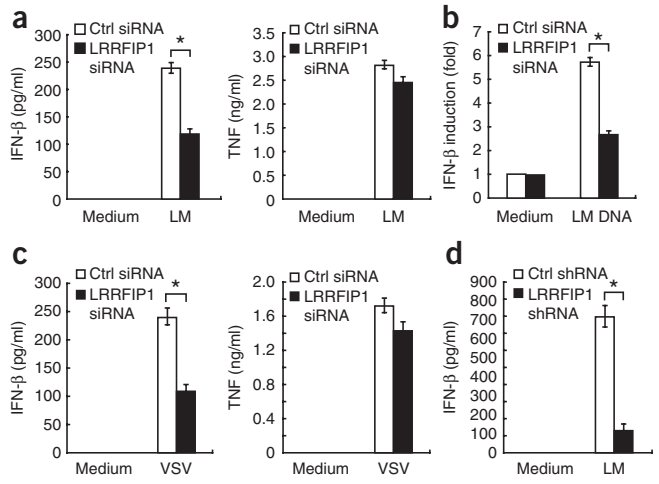

Figure 1 LRRFIP1 increases *L. monocytogenes*– and VSV–induced production of IFN-β in macrophages. (**a**) Enzyme-linked immunosorbent assay (ELISA) of IFN-β and TNF in supernatants of mouse primary peritoneal macrophages transfected for 48 h with LRRFIP1-specific or control (Ctrl) siRNA, then left uninfected (Medium) or infected for 18 h with *L. monocytogenes* (LM) at a multiplicity of infection (MOI) of 100. (**b**) Real-time PCR analysis of IFN-β mRNA expression in RAW264.7 cells transfected for 24 h with LRRFIP1-specific or control siRNA, then left untreated (Medium) or transfected for 4 h with *L. monocytogenes* genomic DNA (5 μg/ml); results are normalized to the expression of HPRT (hypoxanthine guanine phosphoribosyl transferase) and are presented relative to expression in cells transfected with control siRNA and not transfected with genomic DNA, set as 1. (**c**) ELISA of IFN-β and TNF in supernatants of mouse primary peritoneal macrophages transfected for 48 h with LRRFIP1-specific or control siRNA, then infected for 18 h with VSV at an MOI of 10. (**d**) ELISA of IFN-β in RAW264.7 cells with stable knockdown of LRRFIP1 and control RAW264.7 cells left uninfected or infected for 8 h with *L. monocytogenes* (MOI, 100). $*P < 0.01$ (Student's *t*-test). Data are from one experiment of three with similar results (mean ± s.d. of three samples per experiment).

GC-rich Z-form dsDNA such as poly(dG:dC)[19,20]; furthermore, TLR- and MAVS-deficient mouse embryonic fibroblasts and macrophages may produce almost normal amounts of type I interferon after stimulation with B-form DNA[9,22]. Therefore, studies at present indicate that another undefined or unknown cytosolic DNA–sensing system may exist in cells of the immune system to sense random dsDNA molecules by TLR- and RIG-I-independent mechanism[20].

Infection with *Listeria monocytogenes*, which releases dsDNA intracellularly, induces IFN-β production in macrophages in a MAVS- and TLR-independent manner[22,23]. Here we used *L. monoctyogenes* to infect mouse peritoneal macrophages as a model of intracellular pathogen infection of cells to screen for molecules that might mediate cytosolic DNA–induced production of type I interferon. Among the synthetic small interfering RNA (siRNA) molecules tested for leucine-rich repeat (LRR) domain–containing and LRR-interacting proteins, we found that siRNA targeting LRRFIP1 inhibited *L. monocytogenes*–induced production of IFN-β. LRRFIP1 was originally identified as a protein that interacts with the mammalian homolog of *Drosophila* flightless I (Fli-I), a member of the gelsolin family that is important for actin organization during *Drosophila* embryogenesis and myogenesis[24]. LRRFIP1 is localized mainly in the cytoplasm and is able to directly bind dsRNA as well as GC-rich dsDNA[25,26]. Here we show that LRRFIP1 contributed to both *L. monocytogenes*– and VSV-induced production of IFN-β in macrophages. LRRFIP1 increased the expression of IFN-β induced by poly(I:C) dsRNA, as well as that induced by both poly(dA:dT) and poly(dG:dC) dsDNA, which demonstrates that LRRFIP1 can mediate type I interferon responses induced by both B-form and Z-form DNA in addition to sensing dsRNA and RNA viruses. LRRFIP1 bound β-catenin and promoted the activation of β-catenin, which subsequently bound IRF3; this led to more recruitment of p300 acetyltransferase to the IFN-β enhanceosome and resulted in enhanced expression of IFN-β. Notably, the LRRFIP1–β-catenin pathway did not affect PRR-triggered activation of IRF3 and NF-κB but interacted with IRF3 to increase IFN-β expression. Therefore, LRRFIP1 and its downstream partner β-catenin constitute an additional coactivator pathway for IRF3-induced production of type I interferon.

RESULTS

LRRFIP1 increases intracellular pathogen–induced IFN-β

Double-stranded nucleic acids can be introduced into the cytosol of host cells during infection with intracellular pathogens. To screen for cytosolic DNA sensors, we used *L. monocytogenes* as an intracellular pathogen to infect mouse peritoneal macrophages and then used this cell-infection model to screen for molecules that might mediate cytosolic DNA–induced production of type I interferon. We used a synthetic siRNA library for mouse LRR-containing and LRR-interacting proteins in this screen. We transfected mouse primary peritoneal macrophages with individual siRNA molecules in the library and measured IFN-β production induced by *L. monocytogenes* infection. Among the siRNA molecules tested (**Supplementary Table 1**), LRRFIP1-specific siRNA, which inhibited LRRFIP1 mRNA expression (**Supplementary Fig. 1**), was able to suppress *L. monocytogenes*–induced production of IFN-β in mouse primary peritoneal macrophages (**Fig. 1a**). Transfection with LRRFIP1-specific siRNA also inhibited LRRFIP1 mRNA expression in RAW264.7 mouse macrophage cell lines (**Supplementary Fig. 2**). Knockdown of LRRFIP1 inhibited IFN-β mRNA expression induced by transfection with *L. monocytogenes* genomic DNA (**Fig. 1b**), which suggests that LRRFIP1 might increase IFN-β production induced by DNA released by *L. monocytogenes* in macrophages. LRRFIP1 knockdown also inhibited VSV-induced production of IFN-β in primary macrophages (**Fig. 1c**). However, knockdown of LRRFIP1 did not affect the production of tumor necrosis factor (TNF) induced by *L. monocytogenes* or VSV (**Fig. 1a**,**c**). To investigate the role of LRRFIP1 in IFN-β production induced by intracellular pathogens, we also generated RAW264.7 cells with stable knockdown of LRRFIP1 (**Supplementary Fig. 3**). Stable knockdown of LRRFIP1 inhibited about 80% of the *L. monocytogenes*–induced production of IFN-β without affecting TNF production in RAW264.7 cells (**Fig. 1d** and **Supplementary Fig. 4**). However, LRRFIP1 knockdown did not affect LPS-induced production of IFN-β in primary macrophages and RAW264.7 cells (**Supplementary Fig. 5**), which suggests that LRRFIP1 is important for the induction of IFN-β production in macrophages by intracellular pathogens but not by extracellular LPS.

LRRFIP1 increases dsDNA-induced IFN-β expression

Transfection with synthetic analogs of double-stranded nucleic acid can induce considerable IFN-β mRNA expression in RAW264.7 cells. Knockdown of LRRFIP1 inhibited IFN-β mRNA expression induced by the synthetic RNA duplex poly(I:C) and the DNA duplexes poly(dG:dC) and poly(dA:dT) (**Fig. 2a**), which demonstrated that LRRFIP1 contributed to IFN-β expression induced by dsRNA and dsDNA. RNA polymerase III has been shown to be a DNA sensor for B-form DNA but not Z-form DNA[19,20]. Consistent with those studies[19,20], the RNA polymerase III inhibitor ML-60218

© 2010 Nature America, Inc. All rights reserved.

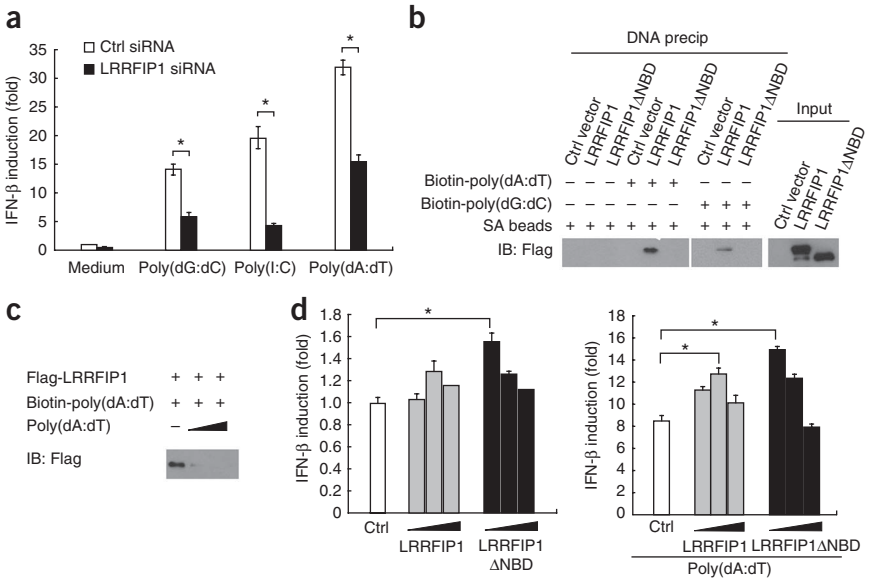

Figure 2 LRRFIP1 increases dsRNA- and dsDNA-induced expression of IFN-β in macrophages. (**a**) Real-time PCR analysis of IFN-β mRNA expression in RAW264.7 cells transfected for 24 h with LRRFIP1-specific or control siRNA, then left untreated or transfected for 4 h with poly(dG:dC) (5.0 μg/ml), poly(I:C) (5.0 μg/ml) or poly(dA:dT) (5.0 μg/ml), presented as described in **Figure 1b**. $^*P < 0.01$ (Student's *t*-test). Data are from one experiment of three with similar results (mean ± s.d.). (**b**,**c**) Immunoblot analysis (IB) of Flag-tagged full-length LRRFIP1 and mutant LRRFIP1ΔNBD precipitated (precip) from HEK293 cells with biotin-conjugated poly(dA:dT) or poly(dG:dC) in the absence (**b**) or presence (**c**) of unconjugated poly(dA:dT) competitor. SA, streptavidin. Data are representative of three experiments. (**d**) Luciferase activity of HEK293T cells transfected with 40 ng IFN-β–luciferase reporter plasmid and 10 ng renilla luciferase plasmid, together with 0 ng, 10 ng, 25 ng or 50 ng (wedges) of plasmid expressing LRRFIP1 or LRRFIP1ΔNBD (equalized with empty control vector (Ctrl)), cultured for 24 h, then left unstimulated (left) or stimulated for 16 h transfection with poly(dA:dT) (2 μg/ml; right); results are presented relative to renilla luciferase activity. $^*P < 0.01$ (Student's *t*-test). Data are from one experiment of three with similar results (mean ± s.d. of four samples).

did not inhibit poly(dG:dC)-induced expression of IFN-β mRNA in RAW264.7 cells (**Supplementary Fig. 6**), which suggests that cytosolic LRRFIP1, but not RNA polymerase III, contributes to the sensing of GC-rich Z-form dsDNA for IFN-β expression.

LRRFIP1 was originally identified as an RNA-binding protein that interacts with human immunodeficiency virus type 1 transactivation-responsive element dsRNA[25]. Meanwhile, another study has reported that LRRFIP1 can bind GC-rich endogenous DNA and function as a transcription factor[26]. We expressed Flag-tagged wild-type LRRFIP1 and mutant LRRFIP1 lacking the N-terminal region containing the putative DNA-binding domain (LRRFIP1ΔNBD) in HEK293 human embryonic kidney cells. Wild-type LRRFIP1 precipitated with exogenous poly(dA:dT) and poly(dG:dC) dsDNA (**Fig. 2b**,**c**). In contrast, the mutant LRRFIP1ΔNBD did not precipitate with the dsDNA, which demonstrated that LRRFIP1 binds dsDNA in an N-terminal region–dependent manner. Overexpression of LRRFIP1ΔNBD alone did increase expression of an IFN-β reporter gene in the HEK293 cells, but overexpression of wild-type LRRFIP1 did not (**Fig. 2d**). However, both wild-type LRRFIP1 and mutant LRRFIP1ΔNBD increased poly(dA:dT)-induced expression of the IFN-β reporter gene in HEK293 cells (**Fig. 2d**). These results suggested that the N-terminal region can regulate the activity of LRRFIP1 to induce IFN-β production.

LRRFIP1 enhances β-catenin activation

IFN-β production is regulated mainly at the transcriptional level. After infection with a pathogen, transcription factors such as IRF3, NF-κB, ATF2 and c-Jun are activated and are recruited to the *Ifnb1* promoter to form the IFN-β enhanceosome and initiate *Ifnb1* transcription[27–29]. To elucidate the mechanism by which LRRFIP1 mediates pathogen-induced production of IFN-β, we observed the effect of LRRFIP1 knockdown on the activation of IRF3 and NF-κB induced by *L. monocytogenes* infection. LRRFIP1-specific siRNA did not inhibit *L. monocytogenes*–induced phosphorylation of IRF3 or the NF-κB subunit p65 in peritoneal macrophages (**Fig. 3a**). The mitogen-activated protein kinases p38 and Jnk mediate activation of ATF2 and c-Jun in pathogen-induced type I interferon responses. However, neither p38 phosphorylation nor Jnk phosphorylation was affected by knockdown of LRRFIP1 (**Fig. 3a**). These data suggested that LRRFIP1 might mediate cytosolic nucleic acid–induced IFN-β expression by regulating the activation of other molecules.

The multifunctional protein β-catenin functions as a coactivator of gene transcription[30]. Studies have shown that LRRFIP1 can interact with β-catenin and increase β-catenin-dependent gene expression[31]. We therefore investigated whether β-catenin is downstream of LRRFIP1 in mediating IFN-β production. We found that β-catenin was translocated to the nucleus after *L. monocytogenes* infection (**Fig. 3b**), which suggested that β-catenin could be involved in the LRRFIP1-mediated production of IFN-β. We examined the interaction between LRRFIP1 and β-catenin in macrophages and found that β-catenin immunoprecipitated together with LRRFIP1 in *L. monocytogenes*–infected macrophages but not in resting macrophages (**Fig. 3c**). In mouse peritoneal macrophages, LRRFIP1-specific siRNA inhibited *L. monocytogenes*–induced phosphorylation of β-catenin at Ser552 (**Fig. 3a**). Similarly, knockdown of LRRFIP1 also inhibited this phosphorylation in VSV-infected macrophages (**Fig. 3d**). However, LRRFIP1-specific siRNA did not affect LPS-induced phosphorylation of β-catenin at Ser552 in primary peritoneal macrophages (data not shown). Consistent with that, stable knockdown of LRRFIP1 greatly inhibited *L. monocytogenes*–induced phosphorylation of β-catenin at Ser552 but failed to inhibit LPS-induced phosphorylation of β-catenin at Ser552 in RAW264.7 cells (**Supplementary Fig. 7**). Together with the results presented above (**Fig. 2**), these results provide evidence that LRRFIP1 functions as a candidate DNA and RNA sensor that increases *L. monocytogenes*– and VSV-induced production of IFN-β, possibly by interacting with β-catenin and promoting β-catenin phosphorylation.

IFN-β production requires β-catenin

To investigate the role of β-catenin in IFN-β production induced by *L. monocytogenes* and VSV, mouse peritoneal macrophages were transfected with β-catenin-specific siRNA to inhibit β-catenin expression (**Supplementary Fig. 8**). Knockdown of β-catenin

© 2010 Nature America, Inc. All rights reserved.

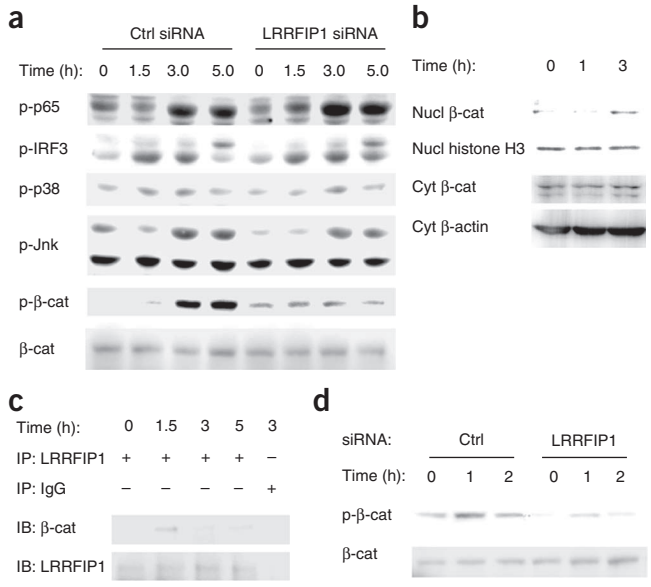

Figure 3 LRRFIP1 mediates *L. monocytogenes*– and VSV-induced activation of β-catenin. (**a**) Immunoblot analysis of phosphorylated (p-) NF-κB p65, IRF3, p38, Jnk and β-catenin (β-cat) in mouse primary peritoneal macrophages infected for various times (above lanes) with *L. monocytogenes* at an MOI of 100. Bottom, total β-catenin (loading control). (**b**) Immunoblot analysis of nuclear (Nucl) and cytoplasmic (Cyt) proteins from RAW264.7 cells infected for various times (above lanes) with *L. monocytogenes* at an MOI of 100; equal amount of proteins were assessed with antibody to β-catenin (anti-β-catenin) and anti–histone H3 (nuclear) or with anti-β-catenin and anti-β-actin (cytoplasmic). (**c**) Immunoblot analysis of RAW264.7 cells infected for various times (above lanes) with *L. monocytogenes* at an MOI of 100; proteins immunoprecipitated (IP) from lysates with an LRRFIP1-specific antibody or immunoglobulin G (IgG) were detected with anti-β-catenin or anti-LRRFIP1. (**d**) Immunoblot analysis of phosphorylated β-catenin in mouse peritoneal macrophages infected for various times (above lanes) with VSV at an MOI of 50 and treated with control or LRRFIP1-specific siRNA. Bottom, total β-catenin (loading control). Data are from one experiment of three with similar results.

inhibited *L. monocytogenes*–induced production of IFN-β (**Fig. 4a**). Similarly, knockdown of β-catenin also inhibited VSV-induced production of IFN-β (data not shown). Notably, we found that knockdown of β-catenin also inhibited extracellular LPS–induced production of IFN-β in mouse peritoneal macrophages (**Fig. 4b**). Overexpression of β-catenin alone was not efficient in inducing expression of the IFN-β reporter gene in HEK293 cells (data not shown). However, overexpression of β-catenin increased TRIF-induced expression of the IFN-β reporter gene in HEK293 cells (**Supplementary Fig. 9**). Overexpression of β-catenin did not affect expression of the IFN-β reporter gene induced by the adaptor MyD88 in the cells.

In further experiments, we crossed mice with *lox*P-flanked alleles encoding β-catenin with mice expressing Cre recombinase from the promoter of the gene encoding the myxovirus-resistance protein Mx1. We treated the offspring with intraperitoneal injection of poly(I:C) to induce deficiency in the gene encoding β-catenin and then used them to investigate the role of β-catenin in IFN-β production. Poly(I:C) challenge could not induce β-catenin deficiency in the mice that had only *lox*P-flanked β-catenin alleles but did not express Cre recombinase; we used these poly(I:C)-challenged mice as control mice. Peritoneal primary macrophages deficient in β-catenin produced much less IFN-β after challenge with VSV, LPS or poly(I:C) than did control cells (**Fig. 4c**). In contrast, LPS- and poly(I:C)-induced production of TNF was higher in β-catenin-deficient macrophages (**Supplementary Fig. 10**), consistent with a published report showing that β-catenin inhibits bacteria-induced inflammation[32]. These results suggest that β-catenin regulates the production of type I interferon and proinflammatory cytokines differently in macrophages.

As LRRFIP1-deficient mice are unavailable, we used the mice with induced β-catenin deficiency as a model to evaluate the role of the LRRFIP1–β-catenin pathway in antiviral innate immune responses *in vivo*. We challenged the β-catenin-deficient mice and control mice by intravenous injection with VSV. After VSV challenge, serum IFN-β concentrations were much lower in β-catenin-deficient mice than in control mice (**Fig. 4d**). Although 80% of the control mice were alive at 24 h after VSV injection, only 20% of the VSV-infected β-catenin-deficient mice survived (**Fig. 4e**). These results suggest that the β-catenin-dependent pathway is required for intracellular pathogen–triggered production of IFN-β and subsequent antiviral innate immune responses.

Direct interaction of β-catenin and IRF3

Finally, we investigated the underlying mechanism by which β-catenin increases IFN-β production. The multifunctional protein

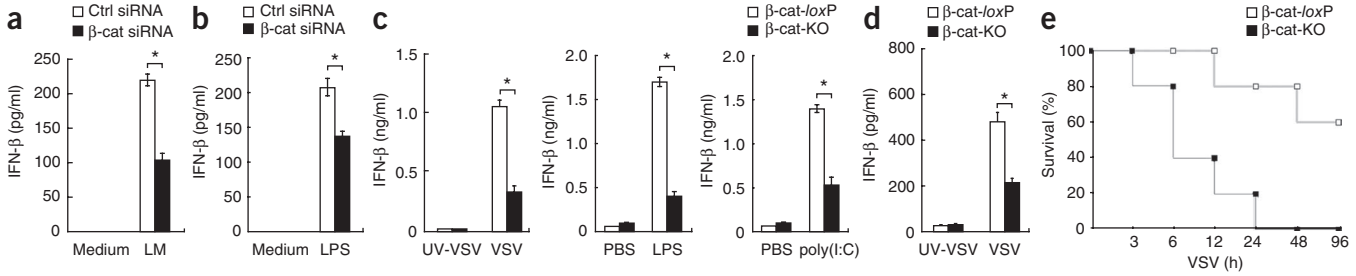

Figure 4 Positive regulation by β-catenin of pathogen-induced production of IFN-β in macrophages. (**a**,**b**) ELISA of IFN-β in supernatants of mouse primary peritoneal macrophages, with (β-cat siRNA) or without (Ctrl siRNA) knockdown of β-catenin, either left untreated (Medium) or infected for 18 h with *L. monocytogenes* (MOI, 100; **a**) or stimulated for 12 h with LPS (100 ng/ml; **b**). (**c**) ELISA of IFN-β in supernatants of primary peritoneal macrophages isolated from β-catenin-deficient mice (β-cat-KO) or control mice (β-cat-*lox*P) and infected for 12 h with VSV (MOI, 10) left untreated (VSV) or treated with ultraviolet irradiation (UV-VSV), or left unstimulated (PBS) or stimulated for 6 h with LPS (100 ng/ml) or poly(I:C) (20 μg/ml). (**d**) ELISA of IFN-β in the serum of β-catenin-deficient or control mice injected intravenously for 6 h with VSV (1×10^6 plaque-forming units/g) with or without ultraviolet irradiation. (**e**) Survival of β-catenin-deficient and control mice ($n = 10$ mice total) injected intravenously with VSV (1×10^7 plaque-forming units/g). *$P < 0.01$ (Student's *t*-test). Data are from one experiment of three with similar results (mean ± s.d. in **a**–**d**).

© 2010 Nature America, Inc. All rights reserved.

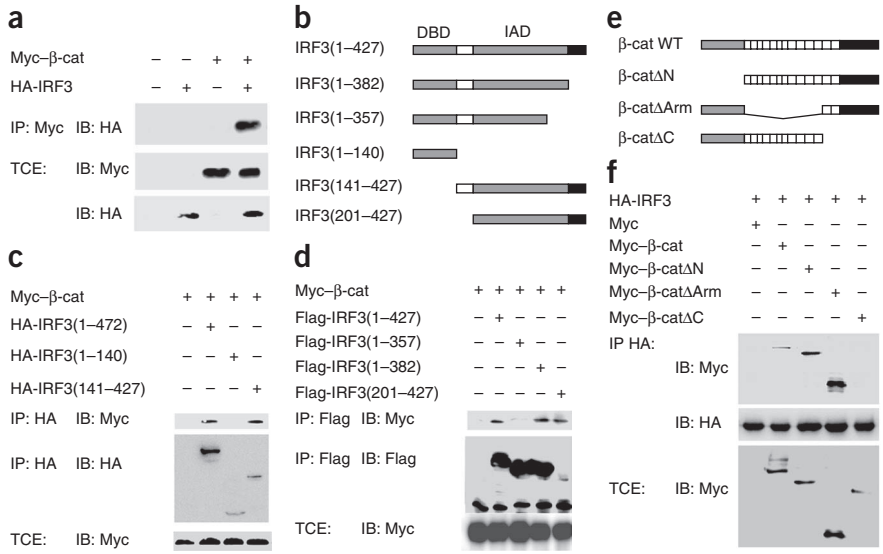

Figure 5 Interaction between β-catenin and IRF3. (**a**) Immunoblot analysis of β-catenin and IRF3 in HEK293T cells cotransfected for 24 h with plasmids for Myc-tagged β-catenin (Myc-β-cat) and hemagglutinin-tagged IRF3 (HA-IRF3); proteins immunoprecipitated from lysates with anti-Myc were detected with anti-hemagglutinin (HA). TCE, immunoblot analysis of total cell extracts. (**b**) IRF3 truncation mutants. Numbers in parentheses indicate amino acids included in construct. DBD (gray box), DNA-binding domain; white box, residues 141–201; IAD (gray box), interaction domain; black box, C terminus. (**c**) Immunoprecipitation and immunoblot analysis of proteins in HEK293T cells transiently transfected with Myc-tagged wild-type β-catenin together with hemagglutinin-tagged wild-type IRF3 (IRF3(1–472)) or the IRF3 truncation mutants in **b**. (**d**) Immunoprecipitation and immunoblot analysis of proteins in HEK293T cells transiently transfected with Myc-tagged wild-type β-catenin together with Flag-tagged wild-type IRF3 or IRF3 truncation mutants. (**e**) β-catenin truncation mutants: β-catΔN lacks the first 140 residues of the N terminus; β-catΔC lacks the final 147 residues of the C terminus; β-catΔArm contains both the N-terminal 140 residues and the C-terminal 147 residues but lacks residues 141–633 in the armadillo domain. (**f**) Immunoprecipitation and immunoblot analysis of proteins in HEK293T cells transiently transfected hemagglutinin-tagged wild-type IRF3 together with Myc-tagged wild-type β-catenin or the truncation mutants of β-catenin in **e**. Data are from one experiment of three with similar results.

β-catenin can interact with transcription factors[30,33]. Given the important role of IRF3 in the production of type I interferon[34], we investigated whether β-catenin positively regulated IFN-β production by interacting with IRF3. Hemagglutinin-tagged IRF3 immunoprecipitated together with Myc-tagged β-catenin (**Fig. 5a**). To map the region of IRF3 that interacted with β-catenin, we constructed a series of hemagglutinin-tagged and Flag-tagged truncation mutants of IRF3 plasmids (**Fig. 5b**). The IRF3 mutant consisting of amino acids 1–141, which contained only the N-terminal DNA-binding domain, lost the ability to bind β-catenin. The mutant IRF3 with truncation of the N-terminal domain (consisting of amino acids 141–472), however, bound β-catenin (**Fig. 5c**), which suggested

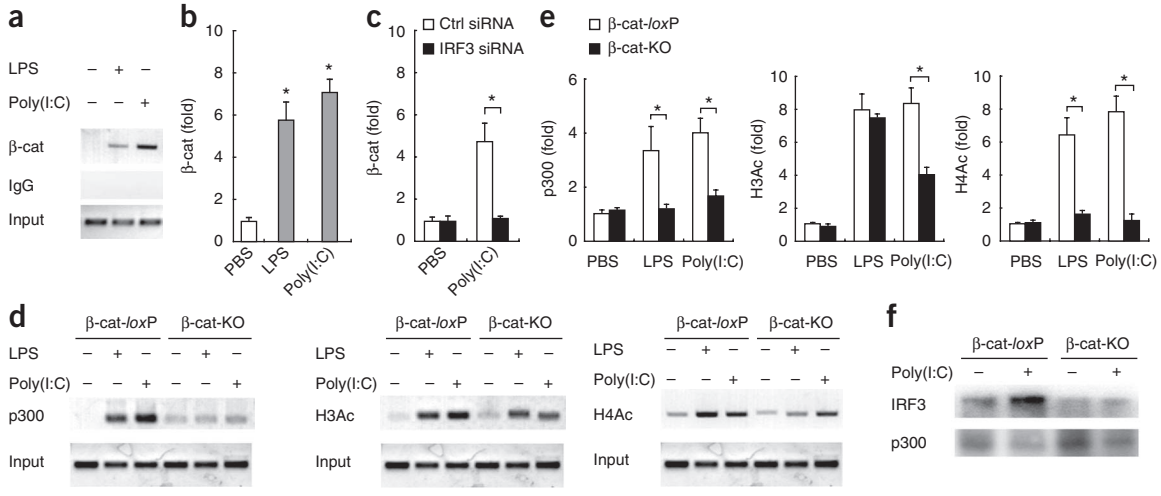

Figure 6 Binding of β-catenin to the *Ifnb1* promoter locus though interaction with IRF3, which promotes p300 recruitment and acetylation of histones H3 and H4 at the *Ifnb1* promoter locus. (**a**,**b**) ChIP analysis of the recruitment of β-catenin to the *Ifnb1* promoter in RAW264.7 cells left unstimulated or stimulated for 1 h with LPS (100 ng/ml) or poly(I:C) (20 μg/ml); *Ifnb1* promoter sequences in input DNA and DNA recovered from antibody-bound chromatin segments were detected by semiquantitive PCR (**a**) or real-time PCR (**b**). (**c**) ChIP analysis of the recruitment of β-catenin to the *Ifnb1* promoter in RAW264.7 cells transfected with control or IRF3-specific siRNA and stimulated as in **a**,**b**; *Ifnb1* promoter sequences were detected by real-time PCR. (**d**,**e**) ChIP analysis of the recruitment of p300 to the *Ifnb1* promoter and acetylation of histones H3 (H3Ac) and H4 (H4Ac) at the *Ifnb1* promoter in β-catenin-deficient (β-cat-KO) and control (β-cat-*lox*P) mouse primary peritoneal macrophages stimulated as in **a**,**b**; *Ifnb1* promoter sequences were detected by semiquantitive PCR (**d**) or real-time PCR (**e**). (**f**) Association of p300 and IRF3 in β-catenin-deficient or control mouse primary peritoneal macrophages stimulated for 1 h with poly(I:C) (20 μg/ml); p300 was immunoprecipitated from nuclear extracts and associated IRF3 was detected by immunoblot. Results in **b**,**c**,**e** were normalized to the corresponding input controls and are presented relative to results obtained with the PBS-treated control. $^*P < 0.01$ (Student's *t*-test). Data are representative of three independent experiments (**a**–**e**; mean and s.e.m. in **b**,**c**,**e**) or are from one experiment of three with similar results (**f**).

© 2010 Nature America, Inc. All rights reserved.

that the C-terminal transactivation domain of IRF3 was required for its interaction with β-catenin. In contrast to the IRF3 mutants containing amino acids 1–382 or 201-427, the IRF3 mutant containing amino acids 1–357 did not efficiently coimmunoprecipitate β-catenin (**Fig. 5d**), which demonstrated that residues 357–382 in the C-terminal domain of IRF3 were necessary for its interaction with β-catenin. We also generated several truncation mutants of β-catenin lacking the first 140 residues of the N terminus or the final 147 residues of the C terminus or containing both the N-terminal 140 residues and the C-terminal 147 residues but lacking residues 141–633 of the armadillo domain (**Fig. 5e**). Among the three mutants, only the mutant lacking the final 147 residues of the C terminus failed to immunoprecipitate together with IRF3 (**Fig. 5f**). These results demonstrate that β-catenin can bind IRF3 transactivation domain through its C-terminal domain.

Enhanced recruitment of p300 to IRF3 by β-catenin

It has been shown that β-catenin can increase target gene transcription by recruiting the histone acetyltransferases p300 and CBP[33]. Both p300 and CBP are recruited to the IFN-β enhanceosome by interacting with IRF3 and synergistically activate *Ifnb1* transcription by promoting hyperacetylation of histones H3 and H4 at the *Ifnb1* promoter[35,36]. Thus, we investigated whether β-catenin has a role in the recruitment of p300 and acetylation of histones H3 and H4 at the *Ifnb1* promoter. To simplify the experimental system, we used poly(I:C) to stimulate macrophages to activate the *Ifnb1* promoter. Chromatin-immunoprecipitation (ChIP) experiments showed that β-catenin was recruited to the *Ifnb1* promoter after stimulation of macrophages with poly(I:C) (**Fig. 6a**,**b**). IRF3-specific siRNA, which efficiently inhibited IRF3 expression (**Supplementary Fig. 11**), greatly inhibited poly(I:C)-induced recruitment of β-catenin to the *Ifnb1* promoter (**Fig. 6c**), which suggested that β-catenin bound to the *Ifnb1* promoter locus by interacting with IRF3. Deficiency in β-catenin significantly inhibited poly(I:C)-induced recruitment of p300 as well as acetylation of histones H3 and H4 in the *Ifnb1* promoter region (**Fig. 6d**,**e**). Similarly, LPS- and poly(I:C)-induced recruitment of p300 and acetylation of histones H3 and H4 in the *Ifnb1* promoter region were lower in β-catenin-deficient macrophages than in control cells (**Fig. 6d**,**e**). These results indicated that β-catenin enhanced acetylation of the *Ifnb1*promoter by promoting recruitment of p300. In support of that hypothesis, poly(I:C)-induced formation of the IRF3-p300 complex was inhibited in β-catenin-deficient macrophages (**Fig. 6f**). Together these results demonstrate that β-catenin interacts with IRF3, facilitates the recruitment of p300 to the *Ifnb1* promoter through IRF3 and subsequently increases hyperacetylation of histones H3 and H4 at the *Ifnb1* promoter, which results in enhanced IFN-β expression.

DISCUSSION

One characteristic of innate immunity is the rapid and efficient detection of invading pathogens through recognition of the PAMPs by host PRRs. After recognizing their corresponding ligands, host PRRs activate distinct signaling pathways that lead to the secretion of type I interferon and proinflammatory cytokines for the initiation of innate immune responses to invading pathogens. Identifying the structural basis for the recognition of PAMPs by PRRs has attracted much attention in recent years. TLRs are transmembrane proteins that contain luminal LRRs and sense the conserved components of invading microbes. TLR3 and TLR9 have been linked to the recognition of dsRNA and dsDNA, respectively. In addition to the nucleic acid–sensing TLRs, many other kinds of PRRs have been identified, including the NLR family (nucleotide-binding domain and LRR), which also contain LRRs. We therefore investigated whether there are other unidentified LRR-containing PRRs or LRR-interacting proteins that may be involved in sensing pathogenic components for initiation of innate immune responses, such as the induction of type I interferon. We found that siRNA targeting LRRFIP1 inhibited *L. monocytogenes*–induced production of IFN-β. We further showed that knockdown of LRRFIP1 also inhibited VSV-induced production of IFN-β. On the basis of that observation, we propose that LRRFIP1 can detect exogenous dsDNA through its nucleic acid–binding domain and increase the production of type I interferon. Therefore, LRRFIP1 is probably an interferon-inducing sensor of nucleic acids.

Stimulation of many cell types with viruses, bacteria and TLR ligands results in the production of type I interferon, which is critical for the antimicrobial response. Factors that interact with IRF3 and the interferon enhanceosome complex have been well characterized. However, how innate sensors detect pathogenic products and initiate the signaling cascades that activate IRF3-dependent production of type I interferon remains incompletely understood. The mechanisms by which cells of the immune system sense VSV and *L. monocytogenes* and induce the production of type I interferon have been studied intensively. VSV-induced production of type I interferon has been demonstrated to depend on RIG-I and MAVS[5,37]; however, induction of type I interferon by dsDNA in primary cells was found to be independent of MAVS. Furthermore, *L. monocytogenes* induces the production of type I interferon through a MAVS-independent pathway[22]. Here we have shown that the dsRNA-binding protein LRRFIP1 contributed to both VSV- and *L. monocytogenes*–induced production of type I interferon. Notably, we have shown that LRRFIP1 bound not only B-form dsDNA but also Z-form dsDNA. These data indicate that LRRFIP1 may contribute to the sensing of a wide variety of intracellular pathogens by detecting dsRNA as well as dsDNA. Therefore, we propose that LRRFIP1-dependent signal transduction is MAVS independent but that it may act together with the MAVS-dependent pathway to more efficiently mediate VSV-induced production of type I interferon. Similarly, as double deficiency in MyD88 and TRIF does not affect *L. monocytogenes*–induced production of type I interferon[23], the positive regulatory role of LRRFIP1 in *L. monocytogenes*–induced production of type I interferon may be also TLR independent. It has been reported that AIM2 deficiency results in lower production of IL-1β but upregulated production of type I interferon after cytosolic DNA challenge or *L. monocytogenes* infection[18]. It remains unclear whether LRRFIP1 and AIM2 affect each other in the context of cytosolic DNA.

RIG-I is one of the main PRRs that sense intracellular dsRNA. The C-terminal portion of RIG-I not only contains the RNA-recognizing domain but also functions as an internal repressor domain that controls multimerization of RIG-I and its interaction with IPS-1; thus, deletion of the RIG-I repressor domain results in constitutive signaling to the *Ifnb1* promoter[38]. Consistent with that, ΔRIG-I, which contains only the N-terminal caspase-recruitment domain of RIG-I, is more efficient than full-length RIG-I in inducing expression of an IFN-β reporter gene when overexpressed alone, and both full-length RIG-I and ΔRIG-I can increase VSV-induced expression of the IFN-β reporter gene[4]. Similarly, we found that overexpression of the mutant LRRFIP1ΔNBD alone induced expression of an IFN-β reporter gene, but overexpression of wild-type LRRFIP1 did not. Meanwhile, both wild-type LRRFIP1 and LRRFIP1ΔNBD increased poly(dA:dT)-induced expression of IFN-β. It remains to be investigated how the LRRFIP1 N-terminal DNA-binding domain regulates LRRFIP1 activity for signaling to the *Ifnb1* promoter. In contrast,

© 2010 Nature America, Inc. All rights reserved.

deletion of the DNA-binding domain of IRF3 selectively and potently inhibits virus-induced activation of the *Ifnb1* promoter[39]. These results suggest that LRRFIP1 might function as a candidate DNA sensor rather than a transcription factor in intracellular DNA–induced IFN-β responses.

In the present study we have linked the β-catenin pathway to induction of the production of type I interferon and antiviral immunity and have also provided a mechanistic explanation for the role of LRRFIP1 in intracellular pathogen–induced production of type I interferon. It is known that β-catenin, the key effector of Wnt signaling, has important roles in cell growth and differentiation in many cell types. It has also been reported that β-catenin is involved in suppressing the replication of human immunodeficiency virus in peripheral blood mononuclear cells[40]. Notably, we found that LRRFIP1 interacted with β-catenin and promoted phosphorylation of β-catenin at Ser552 in pathogen-infected cells. Many amino acid residues of β-catenin are phosphorylated. Phosphorylation at Ser552 promotes the transcriptional activity of β-catenin[41]. Knockdown of β-catenin and deficiency in β-catenin inhibited VSV- and *L. monocytogenes*–induced production of type I interferon, which suggests that LRRFIP1 increases intracellular pathogen–induced production of type I interferon, possibly by promoting β-catenin activation. Although our results showed that LRRFIP1 interacted with β-catenin after pathogen challenge, it remains unclear whether LRRFIP1 directly binds β-catenin and how the interaction promotes β-catenin activation. Notably, although β-catenin also increased LPS-induced production of IFN-β, knockdown of LRRFIP1 did not affect LPS-induced phosphorylation of β-catenin and production of IFN-β, which suggests that these last processes are independent of LRRFIP1. Identifying the pathway that mediates β-catenin activation in response to LPS will be important for elucidating TLR4 signaling mechanisms.

In the present study we found that β-catenin inhibited TLR3- and TLR4-mediated production of TNF but increased TLR3- and TLR4-mediated production of IFN-β in macrophages. Consistent with our results, β-catenin is reported to negatively regulate bacteria-induced inflammation by inhibiting NF-κB activity[32]. Moreover, activating the Wnt pathway is reported to increase H1N1 influenza–induced IFN-β production[42]. Our results have provided a mechanistic explanation for the role of the WNT pathway in virus-induced production of IFN-β.

Unlike TLR3 and TLR4, which mediate IFN-β production through a TRIF-dependent pathway, TLR7, TLR8 and TLR9 mediate IFN-β production through a MyD88-dependent pathway. Overexpression of β-catenin increased TRIF-induced but not MyD88-induced expression of the IFN-β reporter gene in HEK293T cells, possibly because MyD88 induces expression of type I interferon mainly by activating IRF7, which is constitutively expressed in plasmacytoid dendritic cells. The role of β-catenin in TLR7-, TLR8- and TLR9-mediated production of type I interferon in plasmacytoid dendritic cells needs to be investigated further.

Ifnb1 expression is dependent on the assembly of a transcription enhanceosome consisting of many transcription factors. IRF3 is one of the main transcription factors responsible for recruiting the histone acetyltransferases p300 and CBP to the IFN-β enhanceosome[29]. Meanwhile, β-catenin has been demonstrated to upregulate target-gene expression by recruiting p300 and CBP, functioning as coactivator of gene transcription. Our results have shown that the poly(I:C)-induced recruitment of p300 to the *Ifnb1* promoter was interrupted in β-catenin-deficient macrophages. Notably, knockdown of IRF3 inhibited poly(I:C)-induced recruitment of β-catenin to the *Ifnb1* promoter. These data support the hypothesis that β-catenin associates with the IFN-β enhanceosome by interacting with IRF3 and recruits p300 to the *Ifnb1* promoter to increase histone hyperacetylation and transcription of *Ifnb1* in innate immune responses. Given that knockdown of LRRFIP1 inhibited neither phosphorylation of p38 and Jnk nor phosphorylation of IRF3 and NF-κB and that knockdown of IRF3 impaired recruitment of β-catenin to the *Ifnb1* promoter, we propose that LRRFIP1 and downstream β-catenin mediate intracellular pathogen–induced production of type I interferon by acting as a coactivating pathway for such interferon production.

In summary, we have provided evidence here that LRRFIP1 and β-catenin have important roles in both VSV- and *L. monocytogenes*–induced production of IFN-β in macrophages. LRRFIP1 bound exogenous nucleic acid and increased dsRNA- and dsDNA-induced production of IFN-β, which suggests that LRRFIP1 functions as a candidate sensor of dsRNA and dsDNA in intracellular pathogen–induced innate immunity. We have identified β-catenin as downstream signal molecule of LRRFIP1 that positively regulated VSV- and *L. monocytogenes*–induced production of IFN-β. Further experiments indicated that β-catenin also increased production of type I interferon in several PRR pathways, such as the TLR4 and TLR3 pathways. Our results have identified an additional coactivator pathway that senses both cytosolic dsRNA and dsDNA and increases IFN-β expression by promoting IRF3-dependent p300 recruitment and histone hyperacetylation of the *Ifnb1* promoter in intracellular pathogen–induced innate immune responses.

METHODS

Methods and any associated references are available in the online version of the paper at http://www.nature.com/natureimmunology/.

Note: Supplementary information is available on the Nature Immunology website.

ACKNOWLEDGMENTS

We thank X. Ma and T. Zuo for technical assistance; W. Pan (Second Military Medical University) for VSV; and H. Shen (University of Pennsylvania School of Medicine) for *L. monocytogenes*. Supported by the National Natural Science Foundation of China (30825036 and 30721091), the National Key Basic Research Program of China (2007CB512403), the National Grand Program on Key Infectious Disease (2009ZX10004-309) and the Program for New Century Excellent Talents in University of the Ministry of Education of China (NCET-07-0143).

AUTHOR CONTRIBUTIONS

P.Y., H.A., X.L., M.W., Y.Z. and Y.R. did the experiments; and X.C. and H.A. designed the study and wrote the paper.

COMPETING FINANCIAL INTERESTS

The authors declare no competing financial interests.

Published online at http://www.nature.com/natureimmunology/.
Reprints and permissions information is available online at http://npg.nature.com/reprintsandpermissions/.

1. Takeda, K., Kaisho, T. & Akira, S. Toll-like receptors. *Annu. Rev. Immunol.* **21**, 335–376 (2003).
2. O'Neill, L.A. & Bowie, A.G. The family of five: TIR-domain-containing adaptors in Toll-like receptor signalling. *Nat. Rev. Immunol.* **7**, 353–364 (2007).
3. Alexopoulou, L., Holt, A.C., Medzhitov, R. & Flavell, R.A. Recognition of double-stranded RNA and activation of NF-κB by Toll-like receptor 3. *Nature* **413**, 732–738 (2001).
4. Yoneyama, M. *et al.* The RNA helicase RIG-I has an essential function in double-stranded RNA-induced innate antiviral responses. *Nat. Immunol.* **5**, 730–737 (2004).
5. Kato, H. *et al.* Differential roles of MDA5 and RIG-I helicases in the recognition of RNA viruses. *Nature* **441**, 101–105 (2006).
6. Hiscott, J., Lin, R., Nakhaei, P. & Paz, S. MasterCARD: a priceless link to innate immunity. *Trends Mol. Med.* **12**, 53–56 (2006).
7. Pichlmair, A. *et al.* RIG-I-mediated antiviral responses to single-stranded RNA bearing 5′-phosphates. *Science* **314**, 997–1001 (2006).

© 2010 Nature America, Inc. All rights reserved.

8. Kato, H. *et al.* Length-dependent recognition of double-stranded ribonucleic acids by retinoic acid-inducible gene-I and melanoma differentiation-associated gene 5. *J. Exp. Med.* **205**, 1601–1610 (2008).
9. Ishii, K.J. *et al.* A Toll-like receptor-independent antiviral response induced by double-stranded B-form DNA. *Nat. Immunol.* **7**, 40–48 (2006).
10. Takaoka, A. *et al.* DAI (DLM-1/ZBP1) is a cytosolic DNA sensor and an activator of innate immune response. *Nature* **448**, 501–505 (2007).
11. Burckstummer, T. *et al.* An orthogonal proteomic-genomic screen identifies AIM2 as a cytoplasmic DNA sensor for the inflammasome. *Nat. Immunol.* **10**, 266–272 (2009).
12. Hornung, V. *et al.* AIM2 recognizes cytosolic dsDNA and forms a caspase-1-activating inflammasome with ASC. *Nature* **458**, 514–518 (2009).
13. Fernandes-Alnemri, T., Yu, J.W., Datta, P., Wu, J. & Alnemri, E.S. Aim2 activates the inflammasome and cell death in response to cytoplasmic DNA. *Nature* **458**, 509–513 (2009).
14. Roberts, T.L. *et al.* HIN-200 proteins regulate caspase activation in response to foreign cytoplasmic DNA. *Science* **323**, 1057–1060 (2009).
15. Ishii, K.J. *et al.* TANK-binding kinase-1 delineates innate and adaptive immune responses to DNA vaccines. *Nature* **451**, 725–729 (2008).
16. Wang, Z. *et al.* Regulation of innate immune responses by DAI (DLM-1/ZBP1) and other DNA-sensing molecules. *Proc. Natl. Acad. Sci. USA* **105**, 5477–5482 (2008).
17. Fernandes-Alnemri, T. *et al.* The AIM2 inflammasome is critical for innate immunity to *Francisella tularensis*. *Nat. Immunol.* (2010).
18. Rathinam, V.A. *et al.* The AIM2 inflammasome is essential for host defense against cytosolic bacteria and DNA viruses. *Nat. Immunol.* (2010).
19. Chiu, Y.H., Macmillan, J.B. & Chen, Z.J. RNA polymerase III detects cytosolic DNA and induces type I interferons through the RIG-I pathway. *Cell* **138**, 576–591 (2009).
20. Ablasser, A. *et al.* RIG-I-dependent sensing of poly(dA:dT) through the induction of an RNA polymerase III-transcribed RNA intermediate. *Nat. Immunol.* **10**, 1065–1072 (2009).
21. O'Neill, L.A. DNA makes RNA makes innate immunity. *Cell* **138**, 428–430 (2009).
22. Sun, Q. *et al.* The specific and essential role of MAVS in antiviral innate immune responses. *Immunity* **24**, 633–642 (2006).
23. Stetson, D.B. & Medzhitov, R. Recognition of cytosolic DNA activates an IRF3-dependent innate immune response. *Immunity* **24**, 93–103 (2006).
24. Liu, Y.T. & Yin, H.L. Identification of the binding partners for flightless I, a novel protein bridging the leucine-rich repeat and the gelsolin superfamilies. *J. Biol. Chem.* **273**, 7920–7927 (1998).
25. Wilson, S.A., Brown, E.C., Kingsman, A.J. & Kingsman, S.M. TRIP: a novel double stranded RNA binding protein which interacts with the leucine rich repeat of flightless I. *Nucleic Acids Res.* **26**, 3460–3467 (1998).
26. Suriano, A.R. *et al.* GCF2/LRRFIP1 represses tumor necrosis factor α expression. *Mol. Cell. Biol.* **25**, 9073–9081 (2005).
27. Thanos, D. & Maniatis, T. Virus induction of human IFN β gene expression requires the assembly of an enhanceosome. *Cell* **83**, 1091–1100 (1995).
28. Falvo, J.V., Parekh, B.S., Lin, C.H., Fraenkel, E. & Maniatis, T. Assembly of a functional beta interferon enhanceosome is dependent on ATF-2-c-jun heterodimer orientation. *Mol. Cell. Biol.* **20**, 4814–4825 (2000).
29. Wathelet, M.G. *et al.* Virus infection induces the assembly of coordinately activated transcription factors on the IFN-β enhancer in vivo. *Mol. Cell* **1**, 507–518 (1998).
30. Stadeli, R., Hoffmans, R. & Basler, K. Transcription under the control of nuclear Arm/β-catenin. *Curr. Biol.* **16**, R378–R385 (2006).
31. Lee, Y.H. & Stallcup, M.R. Interplay of Fli-I and FLAP1 for regulation of beta-catenin dependent transcription. *Nucleic Acids Res.* **34**, 5052–5059 (2006).
32. Duan, Y. *et al.* β-Catenin activity negatively regulates bacteria-induced inflammation. *Lab. Invest.* **87**, 613–624 (2007).
33. Mosimann, C., Hausmann, G. & Basler, K. β-catenin hits chromatin: regulation of Wnt target gene activation. *Nat. Rev. Mol. Cell Biol.* **10**, 276–286 (2009).
34. Taniguchi, T., Ogasawara, K., Takaoka, A. & Tanaka, N. IRF family of transcription factors as regulators of host defense. *Annu. Rev. Immunol.* **19**, 623–655 (2001).
35. Parekh, B.S. & Maniatis, T. Virus infection leads to localized hyperacetylation of histones H3 and H4 at the IFN-β promoter. *Mol. Cell* **3**, 125–129 (1999).
36. Merika, M., Williams, A.J., Chen, G., Collins, T. & Thanos, D. Recruitment of CBP/p300 by the IFN-β enhanceosome is required for synergistic activation of transcription. *Mol. Cell* **1**, 277–287 (1998).
37. Kumar, H. *et al.* Essential role of IPS-1 in innate immune responses against RNA viruses. *J. Exp. Med.* **203**, 1795–1803 (2006).
38. Saito, T. *et al.* Regulation of innate antiviral defenses through a shared repressor domain in RIG-I and LGP2. *Proc. Natl. Acad. Sci. USA* **104**, 582–587 (2007).
39. Karpova, A.Y., Ronco, L.V. & Howley, P.M. Functional characterization of interferon regulatory factor 3ª (IRF-3ª), an alternative splice isoform of IRF-3. *Mol. Cell. Biol.* **21**, 4169–4176 (2001).
40. Kumar, A. *et al.* Active beta-catenin signaling is an inhibitory pathway for human immunodeficiency virus replication in peripheral blood mononuclear cells. *J. Virol.* **82**, 2813–2820 (2008).
41. Fang, D. *et al.* Phosphorylation of β-catenin by AKT promotes β-catenin transcriptional activity. *J. Biol. Chem.* **282**, 11221–11229 (2007).
42. Shapira, S.D. *et al.* A physical and regulatory map of host-influenza interactions reveals pathways in H1N1 infection. *Cell* **139**, 1255–1267 (2009).

© 2010 Nature America, Inc. All rights reserved.

ONLINE METHODS

Mice and reagents. C57BL/6 mice (Joint Ventures Sipper BK Experimental Animal Company) were used at the age of 4–6 weeks. Transgenic mice expressing Cre recombinase under control of the interferon-inducible *Mx1* promoter (Mx-Cre) were crossed with mice in which essential portions of the gene encoding β-catenin were flanked by *lox*P sequences (*Ctnnb1*$^{fl/fl}$ mice; The Jackson Laboratory). *Ctnnb1*$^{fl/fl}$ mice and Mx-Cre × *Ctnnb1*$^{fl/fl}$ mice were treated with five intraperitoneal injections of 250 μg poly(I:C) (Amersham) at 2-day intervals to induce *Ctnnb1*-deficient mice[43]. Then, 4 d after the final injection, mice were treated with intraperitoneal injection of thioglycolate to elicit peritoneal macrophages or were used for *in vivo* VSV infection as described[44]. *Ctnnb1* in genomes of poly(I:C)-treated *Ctnnb1*$^{fl/fl}$ control mice and Mx-Cre × *Ctnnb1*$^{fl/fl}$ mice was assessed by PCR to confirm that it was deleted in Mx-Cre × *Ctnnb1*$^{fl/fl}$ mice[43]. Poly(I:C)-treated Mx-Cre × *Ctnnb1*$^{fl/fl}$ mice are called 'β-catenin-deficient mice' here; poly(I:C)-treated *Ctnnb1*$^{fl/fl}$ mice served as controls. All animal experiments were undertaken in accordance with the National Institute of Health Guide for the Care and Use of Laboratory Animals with approval of the Scientific Investigation Board of Second Military Medical University. Poly(dG:dC) and poly(dA:dT) (both from Sigma) were purified with Endotoxin Removal Solution (Sigma). Genomic DNA of *L. monocytogenes* was prepared with a DNeasy Tissue kit (Qiagen) and was purified with Endotoxin Removal Solution. Anti-LRRFIP1 (sc-135910), anti-β-catenin (sc-7963) and horseradish peroxidase–coupled secondary antibodies (sc-2030 and sc-2031) were from Santa Cruz Biotechnology. Antibodies specific for phosphorylated IRF3 (4947), β-catenin phosphorylated at Ser552 (9566), phosphorylated p38 (9211), phosphorylated Jnk (9251), phosphorylated NF-κB p65 (3037), hemagglutinin (6E2) and histone H3 (2650) (for immunoblot of total nuclear histone H3) were from Cell Signaling Technology. Anti-p300 (RW128), anti–histone H3 (06-599; for ChIP assay) and anti–histone H4 (06-598) were from Upstate Biotechnology. Anti-Myc (S1826) was from Clontech and anti-Flag (M2) from Stratagene. LPS and poly(I:C) were from Merck.

Cell culture. The RAW264.7 and HEK293T cell lines were from American Type Culture Collection. Mouse peritoneal macrophages were elicited by thioglycolate before isolation[45]. All cells were cultured in endotoxin-free DMEM with 10% (vol/vol) FCS (Invitrogen).

Plasmid constructs. The plasmid expressing LRRFIP1 was from OriGene. Mutant LRRFIP1ΔNBD with deletion of the N-terminal region containing the putative DNA-binding domain was constructed by PCR with a MutanBEST kit (TaKaRa) and primers 5′-CGCGCGGGCCGCCCGTTTTGC-3′ and 5′-GCCAGTGAAGTGGAGGTGAAAAATGAAATCGTGGCGAATGTGG-3′. Sequences encoding IRF3 were amplified from RAW264.7 mRNA and were cloned into the pCMV-HA plasmid. Sequences encoding β-catenin were amplified from human cDNA and were subcloned into the vector pcDNA3-Myc or pCMV-HA. The IFN-β–luciferase reporter plasmid has been described[45]. The pGFP-V-RS vectors expressing short hairpin RNA targeting mouse LRRFIP1 (5′-AATCTGAGCAAGAGATAACTGCCTTAGAA-3′) and control short hairpin RNA were from OriGene.

RNA-mediated interference. Thioglycolate-elicited mouse peritoneal macrophages were transfected with siRNA (30 nM) through use of INTERFERin reagent (Polyplus Transfection) as described[46]. RAW264.7 cells were doubly transfected with INTERFERin reagent 24 h after the first transfection. In ChIP analyses, RAW264.7 cells were transfected with the Macrophage Nucleofector Transfection kit (Amax). The siRNA sequence 5′-GGACCAGATTCAGGATGTAdTdT-3′ (LRRFIP1-specific siRNA) was used for suppression of endogenous LRRFIP1 expression. A mixture of siRNA (5′-AAGGCTTTTCCCAGTCCTTCA-3′ and 5′-AAGATGATGGTGTGCAAGTG-3′) was used for suppression of endogenous β-catenin expression[47]. The IRF3-specific siRNA 5′-GACGCACAGAUGGCUGACU-3′, as described[48], was synthesized with a Silencer siRNA construction kit (Ambion). The nonsense sequence 5′-TTCTCCGAACGTGTCACGTdTdT-3′ was used as control siRNA. To establish cells with stable knockdown of LRRFIP1, plasmids expressing short hairpin RNA were transfected into RAW264.7 macrophages. Cells positive for green fluorescent protein were sorted by MoFlo (Dako Cytomation) 24 h after transfection. Cells with stable knockdown were selected with puromycin (1 μg/ml) and used for further experiments.

Detection of cytokine production. The concentrations of IFN-β and TNF in culture supernatants were measured with ELISA Kits (R&D Systems).

RNA quantification. Total RNA was extracted with TRIzol reagent (Invitrogen). A LightCycler (Roche) and a SYBR RT-PCR kit (TaKaRa) were used for quantitative real-time RT-PCR analysis. The primers used for IFN-β analysis have been described[49]. Data were normalized to HPRT expression in each sample. IFN-β mRNA expression in cells transfected with control siRNA was set as 1.

Immunoblot and precipitation assay. Cells were lysed with M-PER Mammalian Protein Extraction Reagent (Pierce) supplemented with a protease inhibitor 'cocktail', and protein concentrations in the extracts were measured by bicinchoninic acid assay. Nuclear protein was prepared with NE-PER Nuclear and Cytoplasmic Protein Extraction Reagent. Equal amounts of extracts were separated by SDS-PAGE and then transferred onto nitrocellulose membranes for blotting with antibodies. DNA precipitation was assayed as described[10]. Lysates of HEK293T cells transiently transfected with Flag-LRRFIP1 or Flag-LRRFIP1ΔNBD plasmid were incubated for 15 min at 25 °C with streptavidin-conjugated magnetic beads. After centrifugation, supernatants were mixed for 20 min at 4 °C with biotin-conjugated poly(dA:dT) or poly(dG:dC), followed by incubation with streptavidin-conjugated magnetic beads. Precipitated mixtures were washed extensively with lysis buffer, separated by SDS-PAGE and analyzed by immunoblot with anti-Flag.

Assay of luciferase reporter gene expression. HEK293T cells were cotransfected with a mixture of luciferase reporter plasmid, the thymidine kinase promoter–renilla luciferase plasmid pRL-TK and various amounts of β-catenin, TRIF, MyD88 or LRRFIP1 constructs through use of the JetPEI transfection reagent (Polyplus Transfection). Luciferase activity in the cells was measured with the Dual-Luciferase Reporter Assay system according to the manufacturer's instructions (Promega). Data were normalized for transfection efficiency by the division of firefly luciferase activity by renilla luciferase activity.

ChIP. These assays were done according to the protocol of the ChIP assay kit (Upstate Biology). Target-gene promoter sequences in both input DNA and recovered DNA immunocomplexes were detected by RT-PCR. Primer pairs specific for the *Ifnb1* promoter region have been described[50]. Data were normalized to the corresponding DNA input control.

Statistical analysis. Statistical significance was determined by Student's *t*-test, with *P* values of less than 0.05 considered statistically significant.

43. Cobas, M. *et al.* β-catenin is dispensable for hematopoiesis and lymphopoiesis. *J. Exp. Med.* **199**, 221–229 (2004).
44. Wang, C. *et al.* The E3 ubiquitin ligase Nrdp1 'preferentially' promotes TLR-mediated production of type I interferon. *Nat. Immunol.* **10**, 744–752 (2009).
45. An, H. *et al.* SHP-2 phosphatase negatively regulates the TRIF adaptor protein-dependent type I interferon and proinflammatory cytokine production. *Immunity* **25**, 919–928 (2006).
46. Hou, J. *et al.* MicroRNA-146a feedback inhibits RIG-I-dependent Type I IFN production in macrophages by targeting TRAF6, IRAK1, and IRAK2. *J. Immunol.* **183**, 2150–2158 (2009).
47. Yun, M.S., Kim, S.E., Jeon, S.H., Lee, J.S. & Choi, K.Y. Both ERK and Wnt/β-catenin pathways are involved in Wnt3a-induced proliferation. *J. Cell Sci.* **118**, 313–322 (2005).
48. Leung, T.H., Hoffmann, A. & Baltimore, D. One nucleotide in a κB site can determine cofactor specificity for NF-κB dimers. *Cell* **118**, 453–464 (2004).
49. An, H. *et al.* Phosphatase SHP-1 promotes TLR- and RIG-I-activated production of type I interferon by inhibiting the kinase IRAK1. *Nat. Immunol.* **9**, 542–550 (2008).
50. Mokrani, H., Sharaf el, D.O., Mansuroglu, Z. & Bonnefoy, E. Binding of YY1 to the proximal region of the murine β interferon promoter is essential to allow CBP recruitment and K8H4/K14H3 acetylation on the promoter region after virus infection. *Mol. Cell. Biol.* **26**, 8551–8561 (2006).

© 2010 Nature America, Inc. All rights reserved.